Sensor development and optimization for a proton exchange membrane fuel cell system in automotive applications

Hanqing Wang, Simon Morando, Arnaud Gaillard, Daniel Hissel

Sensor development and optimization for a proton exchange membrane fuel cell system in automotive applications

Hanqing Wang [a,b,c,*], Simon Morando [d], Arnaud Gaillard [a,b,c], Daniel Hissel [a,c]

[a] Univ. Bourgogne Franche-Comte, 90010, Belfort Cedex, France
[b] University of Technology of Belfort-Montbeliard, 90010, Belfort Cedex, France
[c] FEMTO-ST, FCLAB, CNRS, Belfort, France
[d] Symbio, R&I department, 25550, Bavans, France

A B S T R A C T

This paper is on the subject of sensor development and sensor-set size optimization approaches for Proton Exchange Membrane Fuel Cell (PEMFC) system in Fuel Cell Electric Vehicles (FCEV) applications. Sensors are classified as physical sensors and gas sensors. Physical sensors are used to detect signals (pressure, mass flow, etc.) which are related to PEMFC system operating state and control. Gas sensors consist of the hydrogen leakage detector for safety reasons and the environment sensor system which is built with various gas sensors to detect gas contaminations (CO_x, SO_x, etc.). Depending on the sensor development review and the sensor specifications comparisons, sensors owning low cost, small volume, fast response, high resolution, excellent stability and durability are favored in FCEV applications. Nevertheless, numerous sensors result in the increase of system complexity, cost, and even the reduction of effectiveness for the fuel cell prognostics and health management algorithms. Thus, sensor-set size optimization and capability validation approaches (model-based, data-driven and hybrid) are reviewed in detail. As a result, a sensor-set size optimization framework is proposed. Some future work on fuel cell sensor system development and optimization is also suggested to facilitate the move towards commercialization.

1. Introduction

During the last decade, greenhouse gas emission due to transportation has become one of the most severe trends for our living environment [1]. Hydrogen energy-based technologies are more and more regarded as perfect solutions. Fuel Cell Electric Vehicles (FCEVs), which are based on Proton Exchange Membrane Fuel Cells (PEMFCs), are already commercialized and treated as an extremely promising and environmentally friendly technology to change the current

* Corresponding author. Univ. Bourgogne Franche-Comte, 90010, Belfort Cedex, France.
E-mail address: hanqing.wang@utbm.fr (H. Wang).

Abbreviations

ABN	Adaptive Bayesian Network
ANFIS	Adaptive Neuro-Fuzzy Inference System
BBN	Bayesian Belief Network
BILP	Binary Integer Linear Programming
BN	Bayesian Network
EBFS	Exhaustive Brute Force Searching
EWMA	Exponentially Weighted Moving Average
FCEV	Fuel Cell Electric Vehicle
FDA	Fisher Discriminant Analysis
KF	Kalman Filter
KPCA	Kernel Principal Component Analysis
LG	Largest Gap
MDs	Mahalanobis Distances
NLS	Non-linear Least Squares algorithm
PCA	Principle Component Analysis
PEMFC	Proton Exchange Membrane Fuel Cell
SVD	Singular Value Decomposition
SVM	Support Vector Machine
SVR	Support Vector Regression
VAV	Variable Air Volume
WD	Wavelet Decomposition
WFA	Wrapper Feature Selection
WNN	Wavelet Neural Network
WPT	Wavelet Packet Transform

transportation mode [2,3].

Sensors, which are widely used in PEMFC systems of FCEVs, are essential to monitor the fuel cell state and control the system. Meanwhile, sensors are also requested for Prognostics and Health Management (PHM) of PEMFC in order to improve the stability and durability [4].

In this study, sensors of PEMFC systems were divided into physical sensors and gas sensors [4,5]. On the one hand, physical sensors, which reflect the system operating state and relate to the control procedure, are used to detect physicals signals, e.g., pressure, mass flow rate, temperature, relative humidity, etc. Gas sensors are primarily employed for safety reasons [6–8]. On the other hand, various gas contaminations exist, which can result in PEMFC degradation and even lead to irreversible damages to the fuel cell. Jing et al. [9] studied the influences of SO_2 and NO_x led to a fuel cell. Based on the test results, the authors pointed out that in the ambient air, the low-level concentration of contaminations can affect the PEMFC performance. Nagahara et al. [10] also studied the impact of sulfur compounds (SO_2, H_2S) and nitrogen compounds (NO_x, NH_3) to PEMFC. The authors found that sulfur compounds caused most severe performance loss of the fuel cell; however, the cell performance was recoverable by flushing out of sulfate from the catalyst layer with high relative humidity (RH). Cheng et al. [11] reviewed the PEMFC contaminations and highlighted that carbon oxide, especially carbon monoxide (CO), impacted the fuel cell performance significantly. Therefore, the gas contamination sensors system, which is also identified as the environment sensor system of FCEV, attracts more and more attentions of researchers nowadays to help alarm the appearance of gas contaminations and decrease the negative impacts on PEMFC [5].

Sensor selection processes require to make compromise among various sensor specifications that differ a lot in terms of technical and measurement features. For example, the mass flow meter based on the ultrasonic technique has fast response and high accuracy, however, the volume and weight are large [12]. In automotive applications, the mass flow meters owning lightweight and small volume are obviously more suitable [13]. Electrochemical gas sensors own low power consumption and good sensitivity, but the cross-sensitivity is unavoidable [14]. Solid-state gas sensors have a fast response and excellent sensitivity; nevertheless, they are more susceptible to interfere gases [15].

Hence, even the commercialized sensors used in automotive applications and laboratory applications have different requirements, it is also necessary to compare them globally and find out the similarities of developing directions. Furthermore, novel techniques employed by sensor prototypes in-lab are also instructive and meaningful to the future sensor development.

With respect to FCEV application, the literature published by Mao et al. emphasized the significance of sensor-set size optimization for PEMFC systems as it helps to reduce cost and complexity of the system, improve the utilization of detected signals, and optimize the accuracy and effectiveness of PHM for the fuel cells [16–18]. Although the sensor-set size can be optimized, usability and availability are also requested to be verified. The performance prediction and PHM capability are always the validation indexes [19,20]. Typical PHM procedure is illustrated in Fig. 1, which consists of three parts: observe, analyze and act [21]. The observed raw data-sets are used to study failure behaviors (diagnosis) and anticipate failure (prognostics, which is usually represented by Remaining Useful Life (RUL)). Then, decision support can be acted, and mitigation actions can be enabled based on estimated RUL. At last, the useful system life can be increased, and the mission achievement is also ensured. Obviously, the "observe" step influences PHM capability significantly. Sensor-set size optimization helps make a balance between the quantity and the quality of raw data. Thus, the efficiency and accuracy of data acquisition and processing can also be enhanced.

This paper is organized as follows. Section 2 details the classifications of physical sensors and gas sensors in FCEV. The comparison of commercialized sensors and in-lab prototype sensors are addressed. Sensor selection process and sensor locations in PEMFC system are proposed. Section 3 reviews sensor-set size optimization approaches and validation methods thoroughly. A framework of sensor optimization and validation steps is proposed at the end. This paper is concluded in the final section 4.

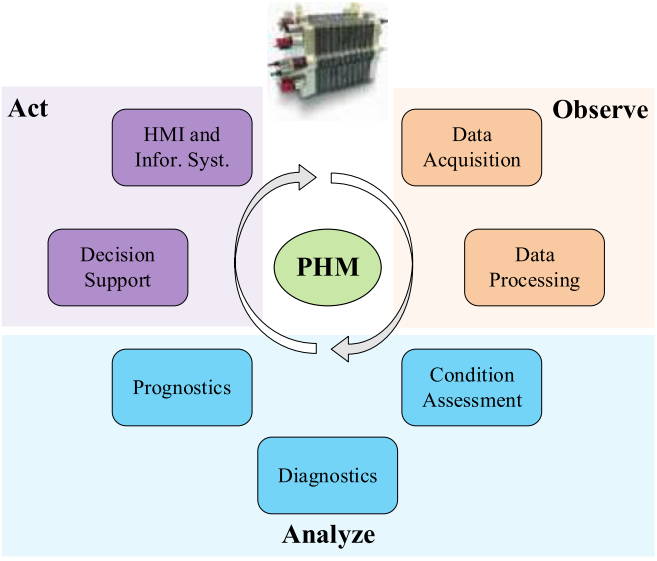

Fig. 1. PHM cycle.

2. Sensor classification

2.1. Physical sensor

Physical sensors for a PEMFC system consist of mass flow rate meter, pressure sensor, temperature sensor and relative humidity sensor. Physical sensors are necessary to be installed in PEMFC systems due to the fact that the physical signals such as hydrogen/air mass flow, coolant temperature and others are closely related to the fuel cell performance monitoring and control. In this study, both commercialized and in-lab developed physical sensors for PEMFC system applications are reviewed in section 2.1.1 and section 2.1.2, respectively. Then, a brief discussion is presented in section 2.1.3.

2.1.1. Commercialized physical sensor

The commercialized physical sensors, which are applied in both automobile industries and laboratory applications, are globally compared in Table .1. The operating principles of different sensors are detailed in the following subsections.

2.1.1.1. Commercialized gas mass flow meter. Air-mass meters applying thermal methods (hot-wire or hot-film air flowmeters) are used which can follow sudden flow changes without mechanically moving parts. The hot-film air-mass meter is a thermal sensor which operates according to the following principle: a centrally situated heating resistor on the measuring cell heats a sensor diaphragm and maintains it at a constant temperature [13,22]. The temperature distribution on the diaphragm is registered by two temperature-dependent resistors which are mounted upstream and downstream of the heating resistor so as to be symmetrical to it. As soon as air flows over the measuring cell, the uniform temperature profile at the diaphragm changes. On the inlet side, the temperature characteristic is steeper since the incoming air flowing past this area cools it off. On the opposite side, the temperature characteristic only changes slightly, because the incoming air flowing past has been heated by the heater element. The change in temperature distribution leads to a temperature difference between the measuring points. The heat dissipated to the air, and therefore the temperature characteristic at the measuring cell is dependent on the air mass flowing past. The temperature difference is a measure of the air-flow mass. It is also direction-dependent so that the air-mass meter can record both the amount and the direction of an air-mass flow. Due to its very thin micromechanical diaphragm, the sensor has a highly dynamic response (<15 ms [13]), a point which is of particular importance when the incoming air is pulsating heavily.

The primary components of the hot-wire air-mass meter are a thermistor, a platinum hot-wire, and an electronic control circuit [13,26]. The thermistor measures the temperature of the incoming air. The hot-wire is maintained at a constant temperature in relation to the thermistor by the electronic control circuit. An increase in air flow will cause the hot-wire to lose heat faster, and the electronic control circuit will compensate by sending more current through the wire. The electronic control circuit simultaneously measures the current flow and puts out a voltage signal in proportion to the current flow [13]. Some of the benefits of a hot-wire and hot-film air-mass meters are: responds very quickly to changes in air flow, low airflow restriction, smaller overall package, less sensitive to mounting location and orientation, etc. However, for the hot-film air-mass meter, the film resistors on the ceramic substrate are exposed to the air mass under measurement. For reasons associated with the flow, this sensor is far less sensitive to contamination than a hot-wire air-mass meter, and there is no need for the ECU to incorporate a self-cleaning burn-off function.

The operating principle of cold-wire Mass Air Flow (MAF) sensor is similar to the hot-wire air-mass meter; however, it uses an additional "cold" resistor to measure the ambient air and provide a reference for the "hot" resistor element used to measure the air flow [54]. The main drawback of the cold-wire air-mass meter is that oil and dirt can coat the MAF sensor and skew its readings.

The Karman Vortex MAF meter always consists of three main parts: vortex generator, mirror (metal foil) and photo coupler (LED and photo transistor) [55]. The intake air flow reacting against the vortex generator creates a swirling effect to the air downstream and this phenomenon is referred to as a "Karman Vortex". The frequencies of the vortices vary in proportion to the intake air velocity. The vortices are metered into a pressure directing hole from which they act upon the metal foil mirror. The air flow against the mirror causes it to oscillate in proportion to the vortex frequency. This causes the illumination from the photo coupler's LED to be alternately applied to and diverted away from a photo transistor. As a result, the photo transistor alternately grounds or opens the voltage signal to the Engine Control Module (ECM). This creates a voltage square wave signal that increases frequency in proportion to the increase in intake air flow. Because of the rapid, high frequency nature of this signal, accurate signal inspection at various engine operating ranges requires using a high quality digital multimeter with frequency capabilities [55].

The H2/Air mass flow meters, which are used for laboratory applications, are always integrated with the mass flow controllers [12,47,48]. The thermal mass flow meters and controllers (for example, the Brooks® Model 5800 series [47]) include the advantages such as excellent signal to noise performance, superior long-term stability, isothermal packaging, wide flow range and fast response performance. The heart of the system is the highly stable sensor which produces an electrical output signal linear with flow rate. The fundamental operating principle of thermal mass flow meters is thermodynamic. A precision power supply directs heat to the midpoint of the sensor tube carrying the flow. On the same tube equidistant upstream and downstream of the heat input, are resistance temperature measuring elements. With no flow, the heat reaching each temperature element is equal. With increasing flow, the flow stream carries heat away from the upstream element and an increasing amount towards the downstream element. An increasing temperature difference develops between the two elements and this difference is proportional to the amount of gas flowing or the mass flow rate. A bridge circuit interprets the temperature difference and an amplifier provides the output to the control circuitry.

For the ultrasonic based mass flow meters (for example, FLEXIM® FLUXUS G809 [12]) are specially designed for the stationary use in hazardous areas and explosive atmospheres. The transducers are mounted on the pipe which is completely filled with the fluid. The ultrasonic signals are emitted alternately by a transducer and received by the other. The physical quantities are determined from the transit times

Table 1
PEMFC system commercialized physical sensor current status.

Property sensed		Automotive industrial application	Laboratorial application
Mass flow rate	H_2/Air	Hot-Film-Meter [13, 22–25]; Hot-Wire-Meter [13, 26–28]; Cold-Wire sensor [29]; Karman Vortex type meter [13,30].	Thermal flow sensor [47]; Based on ultrasonic [12]; MEMS thermal flow sensor [48].
	Liquid coolant	Electromagnetic flow meter [33,34]; Ultrasonic fluid flow sensor [31,32]; Turbine meter [33,35,36].	
Pressure	H_2/Air	Micromechanical based [13]	Micro machined silicon strain gauge based [49].
Temperature	H_2/Air	NTC thermistor [37–39].	PTC or NTC thermistor [39];
	Liquid coolant	PTC or NTC thermistor [39].	Thermocouple [50].
Relative humidity	H_2/Air	Capacitive RH sensor [40–42]; Resistive RH sensor [43–46].	Capacitive RH sensor [51,53].

of the ultrasonic signals. As the fluid where the ultrasound propagates is flowing, the transit time of the ultrasonic signal in flow direction is shorter than the one against the flow direction. The transit time difference is measured and allows the flowmeter to determine the average flow velocity along the propagation path of the ultrasonic signals. A flow profile correction is then performed in order to obtain the area averaged flow velocity, which is proportional to the volumetric flow rate. The integrated microprocessors control the entire measuring cycle. The received ultrasonic signals are checked for measurement usability and evaluated for their reliability. Noise signals are eliminated.

Nowadays, Microelectromechanical Systems (MEMS) flow sensor based thermal gas mass flow meters are developed and commercialized to help users improve quality and save energy. The features of the MEMS flow sensor are: ultra-miniature structure, high resolution, high speed response, wide range, high repeatability, symmetric structure measures reverse flow as well, unaffected by changes in pressure and temperature [48]. The operating principle of a MEMS thermal flow sensor is that when there is no gas flow, the temperature distribution around the heater is symmetric. When gas starts to flow, the temperature upstream of the heater begins to decrease, while the temperature downstream increases, causing a distortion of the symmetric temperature distribution. This temperature difference causes a difference in resistance in a temperature sensor (a thin platinum film) and is used to calculate the mass flow rate (flow rate multiplies density).

2.1.1.2. Commercialized liquid mass flow meter. Electromagnetic flow meter is designed for the measurement of engine coolant flow [33,34]. The flow meters own small footprint, lightweight and are ideal for on board automotive applications where accuracy, zero pressure drop and no moving parts are essential requirements. The electromagnetic flow meter bases its operation on the Faraday Principle, by which a conductor crossing a magnetic field generates a potential. The resultant potential is directly proportional to the flow velocity.

The operating principle of ultrasonic fluid flow meter is similar to the ultrasonic based gas mass meter. The main advantages of ultrasonic fluid flow meter are compact size, no moving parts, lightweight, high accuracy, repeatable and fast response for dynamic flows [31,32].

Turbine flow meter is provided in automotive application measuring coolant flow in engines [33,35,36]. The commercialized turbine meters feature high accuracy and repeatability, compact size, and fast speed of response. However, auxiliary electronic devices are requested for measurements where temperature changes during the test.

2.1.1.3. Commercialized pressure sensor. In automotive application, the Manifold Air Pressure (MAP) are commonly measured based on micromechanical pressure sensors for engine-management systems [13]. Micromechanical pressure sensors determine the absolute pressure of gases by measuring the pressure differential in relation to a reference vacuum. The operating principle of the micromechanical pressure sensors is that the diaphragm of the sensor cell is deflected to varying degrees depending on the voltages across them. This leads to a change in the measurement voltage. This as yet unamplified voltage is, therefore, a measure of the pressure applied to the diaphragm. The Wheatstone bridge circuit is used to obtain higher measurement voltage permitting a higher sensor sensitivity. The signal-conditioning electronic circuitry is integrated on the chip to amplify the bridge voltage, compensate for temperature influences, and linearize the pressure curve. The output voltage is supplied via electrical connections to the engine control unit. The control unit uses this output voltage to calculate the pressure.

A number of current transducers rely on technologies that have problems with zero and span drift, thermal shift, and case stress. According to Ref. [49], micro machined silicon strain gauges that are ultra-stable and suitable for high purity and ultra-high purity requirements. A design feature for controlling stress is the use of dual paired gauges. By using two paired gauges in Wheatstone bridge circuitry, pressure signal is maximized enhancing stability. A key step for eliminating machining stress in the diaphragm is the glass fusion process used to bond the strain gauges to the sensor diaphragm. By using silicon strain gauge technology and the glass fusion bonding method, there is no stress induced from thermal gradients between structural materials.

2.1.1.4. Commercialized temperature sensor. Positive Temperature Coefficient (PTC) thermistors and Negative Temperature Coefficient (NTC) thermistors are the most common temperature sensors for both the gas and the liquid temperature measurements. PTC thermistors are resistors that have a positive temperature coefficient (of the order of a few ‰/K) [13]. The resistance value increases with rising temperature. PTC thermistors conduct electricity better at low temperatures than at high temperatures. A typical application of PTC thermistors is applied as heater elements for auxiliary heaters. The greater resistance with increasing temperature allows heat output to be adjusted automatically NTC thermistors have a marked negative temperature coefficient. The electrical resistance decreases with increasing temperature. Their temperature coefficients can be as much as −6%/K [13]. The typical application of NTC thermistors is used as temperature sensors.

Thermocouple is an electrical device consisting of two dissimilar electrical conductors forming an electrical junction. Thermocouple produces a temperature-dependent voltage as a result of the thermoelectric effect, and this voltage can be interpreted to measure temperature. Thermocouples are widely applied as temperature sensors with features such as inexpensive, interchangeable and wide range of measuring temperature.

2.1.1.5. Commercialized humidity sensor. The capacitive humidity sensor is a small capacitor consisting of a hygroscopic dielectric material placed between a pair of electrodes [40,41,51]. At normal room temperature, the dielectric constant of water vapor is much larger than the constant of the sensor dielectric material. Therefore, the absorption of moisture by the sensor results in an increase in sensor capacitance. At equilibrium conditions, the amount of moisture present in a hygroscopic material depends on both ambient temperature and ambient water vapor pressure. This is true also for the hygroscopic dielectric material used in the sensor. By definition, relative humidity is a function of both the ambient temperature and water vapor pressure. There is a direct relationship between relative humidity, the amount of moisture present in the sensor, and sensor capacitance. This relationship is at the base of the operation of a capacitive humidity instrument. A capacitance variable humidity sensor element features excellent linearity and is capable of measuring from a relative humidity of 0% RH [56]. However, it has disadvantages such as making circuits highly complex and expensive and requiring regular calibration [57].

In a variable resistance humidity sensor, the resistance of the sensor element changes in response to humidity changes, and the resistance changes are extracted as electrical signals [43,44]. Inside the resistive RH sensor, a noble metal thick film conductor such as gold or ruthenium oxide is printed in a comb shape on an alumina substrate, and it is fired to form electrodes. Next, a polymer material is applied to these electrodes to form a humidity sensing film. The sensing mechanism of the polymer film can be explained by the existence of movable ions that are enabled to move freely through the absorption of water molecules. Namely, it is believed that it treats impedance changes caused by the changes in the number of movable ions as electrical conduction. The resistive RH sensor has disadvantages such as difficulty in performing measurement in the low humidity range (5% RH or lower), difficulty in securing a dynamic range in circuits, and large property fluctuations due to temperature [57,58].

2.1.2. In-lab developed physical sensor

In Table .2, in-lab developed prototype physical sensors, which are

Table 2
PEMFC system in-lab prototype physical sensor development.

Technique	Sensible property quantity	Property type
FBG-based	Single	Temperature [59]; Relative humidity [60]
Flexible MEMS-based	Single	Temperature [62,67]
	Two-in-one	Temperature and relative humidity [64]
	Three-in-one	Temperature, relative humidity and voltage [65]
	Five-in-one (HT-PEMFC)	Temperature, flow, pressure, voltage and current [66]
Micro-thermocouple	Single	Temperature [63]
Film thermocouple	Single (HT-PEMFC)	Temperature [68,69]

based on different novel techniques for PEMFC system, are listed. Due to the fact that temperature and relative humidity distributions are closely related to water management and performance of the fuel cell, the development of relative humidity sensor and temperature sensor are most concerned [61–63,68]. The operating principles of sensors in Table .2 are also detailed.

The in-lab developed physical sensors can be classified as insertion models and embedment models. The insertion models, which are inserted into PEMFC from fuel inlet and outlet channels of bipolar flow plate, are always based on the optical fiber technique, for example, Fiber Bragg Grating (FBG) based sensors [59,60]. Pei et al. [63], Ali et al. [68], and Tang et al. [69] also developed novel thermocouples to study thermal distributions within fuel cell stacks. The embedment models, which are embedded directly in gas inlet and outlet channels during fuel cell stack assembly procedure, are usually based on the MEMS technique, especially the flexible MEMS [62,64–67].

2.1.2.1. FBG-based sensor. A fiber Bragg grating (FBG) is a type of distributed Bragg reflector constructed in a short segment of optical fiber that reflects particular wavelengths of light and transmits all others [70]. The fundamental principle behind the operation of an FBG is Fresnel reflection, where light traveling between media of different refractive indices may both reflect and refract at the interface [71]. When the grating is illuminated with broadband light, the reflected power spectrum has structure caused by interference of the light with the planes of the grating, much like Bragg diffraction. The peak of the spectrum, in this case, occurs at a wavelength corresponding to twice the optical path length between adjacent planes, and is called the Bragg wavelength. When the grating is subjected to mechanical or thermal strain its pitch changes, causing a shift in the Bragg wavelength.

David et al. [59] provided a new application of FBG sensors for the study of temperature distribution inside a PEMFC. The authors locate four FBGs from inlet to outlet on the lands between the flow channels in the cathode collector plate of a single test cell. The operating temperature range of the cell is from 20 °C to 80 °C. According to the results, a relative error which is less than 0.2 °C has been obtained.

David et al. [60] proposed an approach to study the difference of relative humidity inside a fuel cell based on a new FBG sensor. The authors use the hygroscopic expansion and contraction of a polyimide recoated FBG RH sensors. Once the concentration of water vapor surrounding FBG changes, the strain in the fiber changes and causes a shift in the Bragg wavelength of the FBG. The FBG RH sensors are installed at two separate channel and lands in the flow channels of anode and cathode. According to the results obtained by the FBG RH sensors, obvious differences of RH exist between land and channels under dynamic conditions especially on the cathode. The result indicates that the RH measurements in the channels are not enough to infer the membrane hydration degree on the cathode side.

2.1.2.2. Flexible MEMS-based sensor. Lee et al. [62] proposed a flexible micro-temperature sensor on a stainless-steel foil substrate (SS-304 with a thickness of 40 μm) to monitor temperature inside a fuel cell. MEMS-based fabrication technique is used to develop the sensor. Compared with traditional thermocouple, the flexible MEMS sensors own characteristics as small volume, highly sensitive, flexible and strong, ease of mass production, and can be placed anywhere. Lee et al. locate the flexible MEMS temperature sensors on the cathode bipolar plate at both the upstream and downstream side. The experiment results indicate that temperature inside a PEMFC was not stable as measured by a thermocouple.

Wang et al. [67] also studied the temperature distribution inside a fuel cell. The authors use six flexible micro-temperature sensors to measure the temperature distributions of the fuel inlet part, the center area and the outlet region. The temperature distribution is monitored more precisely.

Lee et al. [64] proposed a two-in-one flexible MEMS-based micro sensor aiming at temperature and RH measurements inside a fuel cell. The proposed flexible micro sensor is 2 μm thick. The area of temperature sensor is 180 μm × 180 μm, and 180 μm × 220 μm of the humidity sensor. A flow channel was integrated in a stainless-steel base (SS-304) with micro-channels that are 300 μm wide and 200 μm deep using wet-etching technology. The temperature sensor is a resistance temperature detector (RTD) which has a positive temperature coefficient. The humidity sensor is capacitive-based as the temperature variation affects resistive sensors. The authors install one micro-sensor into the center of MEA to measure precisely the temperature and humidity at various flow channels. At last, the authors indicate that this technique can help provide the optimal operating parameters of fuel cell for improving fuel cell performance.

Lee et al. [65,66] proposed three-in-one (temperature, relative humidity, voltage) and five-in-one (temperature, flow, pressure, voltage, current) flexible micro-sensors successively. The three-in-one micro--sensor is fabricated for PEMFC application and the five-in-one micro--sensor is employed in high-temperature PEMFC (HT-PEMFC) application. Nevertheless, their sensing principles are the same. The micro temperature sensor, whose area is 400 μm × 400 μm, is an RTD and has a PTC. The micro voltage sensor has a sensing area of 200 μm × 200 μm and is a miniaturized voltage probe. The film-type probe is installed inside a fuel cell to ensure the voltage is measured in particular locations. The micro pressure sensor is designed with the capacitive sensing element and with sensing area of 800 μm × 800 μm. The hot-wire micro flow sensor is utilized to monitor the flow inside channels of the fuel cell. The micro current sensor consists of the micro voltage probe (400 μm × 350 μm) and the micro resistance probe (350 μm × 350 μm). The probes are integrated in the thickness of a 40 μm stainless steel sheet. The front-end probe is exposed while the other parts are isolated. Hence, the micro current sensor can detect the current of a particular area.

2.1.2.3. Thermocouple-based sensor. Pei et al. [63] measured temperature mapping by micro-thermocouples which are embedded into the cathode plate of the fuel cell. The temperature distributions of a single cell and complete fuel cell stack are both studied. Pei et al. investigate the temperature distribution characteristic in a 46 cells' PEMFC stack, and four sample cells (1st,11th, 23rd, 46th) are embedded with the micro-thermocouples. For each cell, nine thermocouples (T type) are divided into three groups and installed in the top, middle and bottom of the inlet, respectively. According to the results, Pei et al. indicate that in the stack, the highest temperature and the lowest temperature appear in the bottom-middle and the top-middle of the single cell separately. Furthermore, during the optimal design, especially at the high current densities, the heat exchange between the coolant and the middle bipolar plates should be paid special attention.

Ali et al. [68] proposed a novel technique that Type-T thin film

thermocouples (TFTCs) are fabricated on a Kapton substrate to measure the internal temperature distribution of HT-PEMFC. TFTCs are promising to measure the internal temperature of an operating fuel cell benefitting from the small size, fast response and flexibility in design. Type-T TFTCs are selected as they own the lowest temperature coefficient of resistance and the highest thermal electromotive force. Meanwhile, the operating temperature range of Type-T TFTCs (−200 °C–350 °C) is appropriate for the working temperature range of HT-PEMFC (120 °C–200 °C). The TFTCs are fabricated on a 75 μm thick Kapton foil which is a rectangle. Finally, the sealed TFTCs are embedded between the flow plate and the MEA (Celtic® P-1000). Five Type-T TFTCs are used to measure the temperature in the four corners and the center. According to the results, the TFTCs, which own stable performance, are embedded with minimal interference to the performance of the fuel cell. This novel manufacturing technique provides new ways for in situ temperature measurements for fuel cells.

Tang et al. [69] also used Type-T TFTCs to monitor the temperature distribution inside PEMFC. The authors fabricate 25 μm thick Type-T TFTCs by MEMS. The hot junction size of TFTC is selected as 100 μm × 100 μm to obtain enough resolution and durability. Eight TFTCs are embedded between the flow field plate and the MEA to measure the internal temperature distribution of the cell. Finally, Tang et al. state that more frequent temperature fluctuation occurs at the position closer to the bottom of the flow field plate.

2.1.3. Discussion

Although the application fields are different, similarities still exist in commercialized physical sensors. Firstly, the operating temperature limitation of sensors must satisfy the operating temperature range. PEMFC operating temperature is in the range of 50–90 °C. Nowadays, FCEVs are also required to operate at cold environment. To meet the requirements, manufacturers also developed physical sensors which can hold the crucial working conditions. For example, the hot-film based mass air flow meter developed by Bosch can operate in the temperature range from −40 °C to 120 °C [13]. Secondly, thermistor-based temperature sensors are widely selected to detect coolant temperature and gas temperature for both applications. The thermistor-based sensors feature advantages such as low cost, relative high accuracy, linear with temperature change, etc. [39]. Sometimes thermocouple temperature detectors are also selected for the laboratory applications [50]. Thirdly, capacitive relative humidity sensors are widely used for both applications. At last, for relative humidity sensors and temperature sensors, the time constant sometimes is possible to be big, e.g., 5 s [52]. However, too slow response can result in testing errors and make it difficult to develop fuel cell model with high precision [42,43,51].

The differences are mainly important in mass flow meters and pressure sensors. For the automotive industrial application, the sensor elements are much simple and build with fewer auxiliary components [13,24,39]. The control part is embedded in an engine control unit (ECU) which is a separate device. The packages of sensors are mostly industrial plastic and, in this way, the weight and costs can be reduced. The most important characteristics are stability, durability and accuracy for the sensors which are used in automotive applications. For the laboratory applications, the sensor elements are more complicated and always comprise several components [48]. The controllers are always integrated with the sensor elements and operate as the whole [12]. The packages are usually in steel; hence, the weight, volume and cost are increased. The most important characteristics are here response time, resolution and sensitivity for the sensors which are applied in the laboratorial application.

According to the comparative study, the miniaturization of physical sensors is a trend as it can help to improve the compactness of the sensor system. Meanwhile, all-in-one sensors are favored to reduce the complexity of the system.

2.2. Gas sensor

2.2.1. Hydrogen leakage detector (safety reason)

Hydrogen leakage detectors are essential to be fitted on FCEVs for the safety concern by reason of the combustibility of hydrogen. The locations of hydrogen detectors in Honda Clarity FCEV and Toyota Mirai are presented as examples in Fig. 2.

In Honda Clarity FCEV, four hydrogen sensors are present: three sensors inside the motor room, and one inside the filling lid [6]. On the other hand, two hydrogen detectors are fitted with Toyota Mirai: one detector inside the motor room, and the other inside the filling nozzle [7]. Once a potentially hazardous leakage is detected, the hydrogen flow from the tank will be stopped automatically by the system controller [6].

The hydrogen detector of Toyota Mirai is developed by FIS Inc., a group company of Nissha Printing Co., Ltd. The developed catalytic combustion sensors detect any hydrogen leaks within 1 s before the fuel cell vehicle starts up. Meanwhile, the coil-shaped sensing element maximizes the catalyst surface area and extends the sensor's service life [7]. The new compact sensing element detects rises in combustion temperature caused by contact between the catalyst electrodeposited on the platinum wire and the hydrogen. The establishment method of the electrodeposition resolves the conflicts of minimizing size and maximizing catalyst surface area, fast detection and long durability. The hydrogen sensors are also widely developed for in-lab use and based on different techniques: solid-state hydrogen sensor, nano-material based hydrogen sensor, optical hydrogen sensor, MEMS based hydrogen sensor, etc. [8]. The operating principles of these gas sensors will be detailed in the following part.

No matter in real FCEV application or in laboratory study, the requirements of hydrogen leakage sensors are the same: fast response, high resolution, excellent stability and durability.

2.2.2. Gas contaminations of PEMFC

The contaminations of PEMFC can be caused by impurities in hydrogen fuel and air feed streams into anodes and cathodes of fuel cells [11]. The impurities can result in stack performance degradation, and sometimes lead permanent damage to the membrane electrode assemblies (MEA). In Table .3, different gas contaminations sources and their impacts on PEMFC are listed out [9,90–93].

The hydrogen impurities are mainly coming from its manufacturing process. Today, the majority of hydrogen (~95%) is produced from fossil fuels by steam reforming or partial oxidation of methane [84], and only a very small part by other routes such as biomass gasification [85], hydrolysis of sodium borohydride [86] and electrolysis. Hence, the hydrogen production process results in unavoidable impurities such as carbon oxides including CO and CO_2, and sulfur compounds including H_2S and sulfur organics [76]. Moreover, the use of ammonia as a tracer gas in natural gas distribution systems can result in NH_3 impurity (at a level of few ppm (parts-per-million)) in the reformate gas [83].

Chugh et al. [87] experimentally studied and identified the impact of impurities present in refinery hydrogen on PEMFC performance. High level of CO (~80 ppm) was detected in refinery hydrogen, and according to the experiment results, even 10 ppm of CO in hydrogen fuel led to almost 30% voltage loss after an operation of 4 h. Rajalakshmi et al. [75] studied the effect of impurities (CO_2 and NH_3) presented in the anode side of PEMFC. The authors found that CO_2 presence in anode gas decreased the performance of PEMFC by up to 10%. The voltage loss caused by CO_2 was recoverable with passing pure hydrogen fuel. Even worse, 20 ppm of NH_3 in anode gas caused the fuel cell permanent failure in a short duration.

Air is the most practical and economical way to feed the cathode side of the fuel cell stack. However, air pollutants, namely nitrogen oxides (NO_x, including NO and NO_2), sulfur oxides (SO_x, including SO_2 and SO_3), carbon oxides (CO_x, including CO and CO_2), ozone, and other organic chemical species (such as benzoic compounds) contaminate the fuel cell, resulting in MEA damage and performance degradation. The

Fig. 2. Hydrogen detectors/sensors locations in the commercialized FCEV: left-side: Honda Clarity FCEV [6]; right-side: Toyota Mirai [7].

Table 3
Different gas contaminations' sources and impacts to PEMFC [11].

Gas	Source	Affect part	Impact
CO	Reformate hydrogen fuel Air pollutant	Catalyst layer [91]	Strongly reduce the surface-active sites used for hydrogen electro-oxidation [72]; Could also significantly affect the cathode performance [73,74].
CO_2	Reformate hydrogen fuel Air pollutant	Catalyst layer [92]	Lead to the stack performance loss especially at higher current densities [75];
H_2S	Reformate hydrogen fuel Air pollutant	Catalyst layer [93]	Degrade the cell performance significantly through the poisoning effect of the Pt catalysts [76]. Cathode exposure to high concentration hydrogen sulfide can lead to a complete deterioration of cell performance in short period [77].
SO_x	Air pollutant	Catalyst layer [9] Membrane [90]	Lead to "morning voltage drop" in a fuel cell stack and MEA pH be depressed [78]; Make FC current density dropped [79]; Strongly adsorb on the Pt catalyst and be responsible for catalyst poisoning [80]; Lead to difficulties in oxygen reduction [81].
NH_3	Reformate hydrogen fuel Air pollutant	Catalyst layer Membrane [9]	Reduce the proton conductivities of both the Nafion membrane and the anode catalyst ionomer layer [82,83].
NO_x	Air pollutant	Catalyst layer [9]	Lead to "morning voltage drop" in a fuel cell stack and affect the ionomer and/or the catalyst-ionomer interface [78,79]; At the cathode, compete with the oxygen reduction reaction for catalyst active sites [79]; A linear relationship between a cathode Pt catalyst surface coverage and nitric oxide concentration was observed [84].

major sources of these contaminants are the automotive vehicle exhaust and industrial manufacturing processes.

Erbach et al. [88] investigated the influence of operating conditions on CO_2 crossover from fuel cell cathode to anode in an automotive PEMFC system. The automotive full-size fuel cell experiments were carried out on a research platform system for the development of Daimler AG's Mercedes Benz GLC F-Cell. The supplied air at cathode contained 400 ppm of CO_2, and during operation, CO_2 concentrations in the range of 100–200 ppm were monitored on the anode side. CO_2 permeation through membrane reduced the electrochemical active surface area (ECSA) after reduction to CO which absorbs on Pt surface to form Coad. 200 ppm of CO_2 in the anode feed resulted in blocked ECSA of 26% through operation of 24 h. Erbach et al. pointed that a hydrocarbon-based membrane was a better permeation barrier and the system should be operated at low pressures, low relative humidity and low temperatures to minimize the CO_2 crossover to the anode side. For the first time ever, Talke et al. [89] experimentally studied the influence of urban air on automobile fuel cell short stacks with an authentic driving cycle. Tests with a semi-dynamic profile were executed for more than 1560 h and shown an irreversible damage of PEMFC by nitrogen oxides. In some special situations, over 10% power loss occurred for FCEVs in urban areas. Furthermore, even NH_3 only caused a power loss less than 3%, permanent failure was led to the fuel cell.

Therefore, the environment sensor system is promising to be installed on FCEV to detect and analyze the gas contaminations, and improve the fuel cell control systems to avoid fuel cell performance loss, even irreversible damage caused by fuel and gas impurities.

2.2.3. Gas sensor development

As the main elements of environment sensor system for FCEV, gas sensors are highly developed by various techniques and are comparatively presented in Table .4. The operating principles of different gas sensors are detailed and illustrated in Fig. 3.

The electrochemical gas sensors have been developed since 1950s. Electrochemical sensors operate by reacting with the target gas and producing an electrical signal proportional to the gas concentration

Table 4
Comparison of different types of gas sensors.

Sensor type	Principle	Characteristic
Electrochemical	Oxidize the target gas at an electrode [94,96].	➢ Linear output, low power consumption, good resolution, excellent repeatability and accuracy, anti-poison by other gases, low cost [95]. ➢ Cross-sensitivity existence, short shelf life and limited temperature range.
Nondispersive Infrared (NDIR)	Use a broadband lamp source and an optical filter to select the spectral band of target gas [97].	➢ Low energy consumption [98,99]. ➢ Interference, detection limit, large size and high cost [98,100–102].
Solid-State	Measure the change of conductivity as a signal in the presence of target gas [103–106,108,109].	➢ Fast response at high concentration, long life expectancy, versatility [107]. ➢ Susceptible to interference gases [106,107].
Catalytic combustion	Based on the catalytic principle [110].	➢ Detect combustible gases [110]. ➢ Catalyst poisoning, sensor cracking, sensor inhibitors exist [111].
Thermal conductive	Use Wheatstone bridge circuit sense changes in the thermal conductivity and compare it to a reference flow [112].	➢ Bad sensitivity and selectivity [107]; avoid interrupting gas flow when the filament is hot [117].

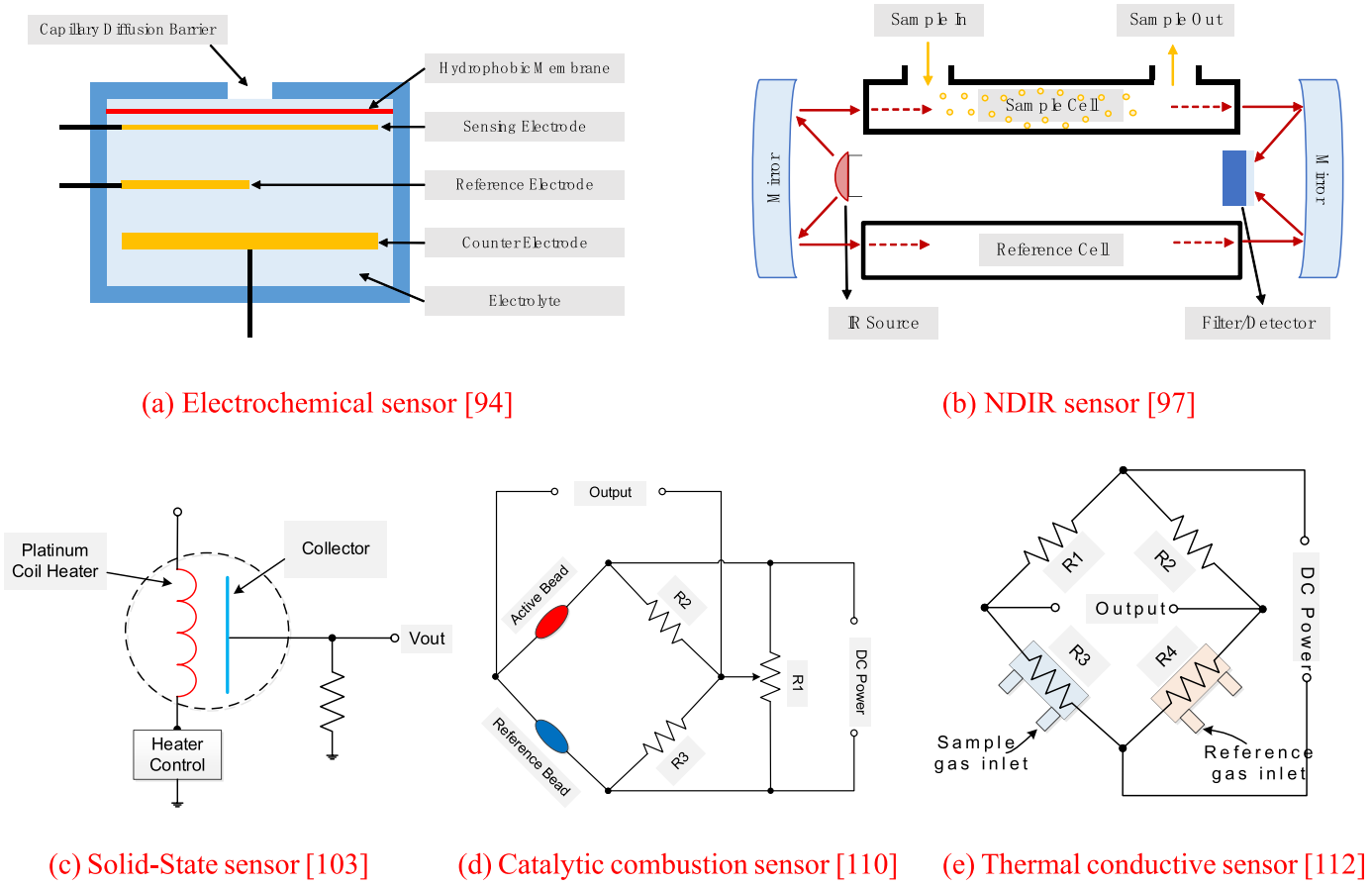

(a) Electrochemical sensor [94]

(b) NDIR sensor [97]

(c) Solid-State sensor [103]

(d) Catalytic combustion sensor [110]

(e) Thermal conductive sensor [112]

Fig. 3. Schematic diagrams of gas sensors operating principles.

[94]. A typical electrochemical sensor consists of a sensing electrode (or working electrode), and a counter electrode separated by a thin layer of electrolyte. Gas that comes in contact with the sensor first passes through a small capillary-type opening and then diffuses through a hydrophobic barrier, and eventually reaches the electrode surface. This approach is adopted to allow the proper amount of gas to react at the sensing electrode to produce a sufficient electrical signal while preventing the electrolyte from leaking out of the sensor. The gas that diffuses through the barrier reacts at the surface of the sensing electrode involving either an oxidation or reduction mechanism. These reactions are catalyzed by the electrode materials specifically developed for the gas of interest. With a resistor connected across the electrodes, a current proportional to the gas concentration flow between the anode and the cathode. The current can be measured to determine the gas concentration. Because current is generated in the process, the electrochemical sensor is often described as an amperometric gas sensor or a micro fuel cell. Although the cross sensitivity unavoidably exists, electrochemical sensors feature some advantages such as linear output, good resolution, excellent repeatability, etc. [96].

NDIR (Non Dispersive InfraRed) gas detection is a well-developed measurement technology. The main advantage is that the detector does not directly react with the target gas. The main components of an NDIR sensor are an infrared detector, an infrared source, an optical filter, and a gas cell or light path. The bandpass filter is important for the selectivity of target gas [97]. The infrared source is directed through the gas cell towards the infrared detector. In parallel, a reference gas cell is required in which filled with a pure target or reference gas. The infrared detector gets its base reading from the reference cell and the gas signal is acquired from the sample cell. According to the Beer-Lambert law, the gas in the cell leads to the absorption of specific wavelengths. Therefore, the gas concentration will be determined by the infrared detector with the measurement of the attenuation of these wavelengths. However, the interference exists due to the spectral aliasing of different gases [98] and there is always a limitation of minimum detection level for NDIR sensor [100].

Solid-state gas sensor always consists of metal oxide or semiconductor, and measure the change of conductivity once the target gas presents [103,104]. A solid-state sensor consists of one or more metal oxides from the transition metals, such as tin oxide, aluminum oxide, etc. There are two common ways of fabricating solid-state sensors: bead-type sensor and chip-type sensor. The metal oxides are processed into a paste to fabricate the bead-type sensor. On the other hand, the metal oxides are vacuum deposited onto a silica chip in order to generate the chip-type sensor. Due to that the made-up solid-state sensors display different gas response characteristics at various temperature ranges, a heating element is essential to be integrated with the solid-state sensor to regulate the sensor temperature. Different heating elements exist, such as the platinum alloy wire, the resistive metal oxide, the thin layer of deposited platinum, etc. During the operation, the solid-state sensor will be heated to a specific high temperature to realize the detection of the target gas. Once the target gas occurs, the gas will be dissociated into charged ions resulting in the transfer of electrons. A pair of biased electrodes are embedded into the metal oxides to detect its conductivity change. The changes in the conductivity of the sensor are measured as a signal. High sensitivity and fast response are the main advantages of the solid-state gas sensor [105]. Nevertheless, solid-state sensors are more susceptible to interference gases than other types of sensors [106,107]. A heating element is also essential to be integrated with the sensing element as solid-state sensors feature different gas response characteristics at different temperature ranges.

Catalytic combustion sensors are primarily used to detect combustible gases [110]. Combustible gas mixtures will burn or ignite below

their ignition temperatures if certain chemical medias present. The specific phenomenon is known as the catalytic combustion, which is the basic operating principle of the catalytic combustion gas sensors [110]. Many metal oxides and their compounds own catalytic properties. Platinum compound is one of the most excellent catalysts for combustion and is widely used in the automobile exhaust system. The Wheatstone bridge circuits are commonly used to measure the output of catalytic sensors. Several drawbacks exist for catalytic combustion sensors, for example, the possibility of catalyst poisoning [111]. Hydrogen, which is the fuel of PEMFC, is a typical combustible gas and as stated previously, the catalytic combustion sensors are used in real FCEVs to detect the hydrogen leak.

Thermal conductive sensors are used to quantify gas concentrations based on varying thermal conductivities of the target gases corresponding to the reference gas [112]. The temperature can affect the thermal conductivity of gas strongly. A Wheatstone bridge circuit is established inside the sensor and is supplied with a constant voltage. The sensing element is open to the atmosphere under test and the reference element is supplied sealed in reference air. The response of the devices depends on the difference between the thermal conductivity of the atmosphere under test and the reference air. The sensitivity and selectivity of this kind of gas sensor are poor [107].

2.2.4. Gas sensor characteristics comparison

In order to compare the characteristics of various gas sensors, the explanations of some main specifications are presented at first.

- Response time [113].

Technically, response time is the time of a sensor or a detector takes to react to a given input. For gas sensors, the target gas is the input. Sensors combined with fast response capabilities are more welcomed no matter for in-situ applications or real industrial applications. For example, in FCEV, hydrogen leakage detectors are requested responding quickly enough to avoid dangerous situations since hydrogen is inflammable gas. Gas sensor response time is commonly united by seconds and is always represented by the time it takes to display 90% of the actual concentration (t_{90} time).

- Resolution [114].

Resolution is the minimum amount of change of a specimen under test that a sensor can measure. Resolution is also known as the capability of measuring the minimum increment. Typically, sensors should have a resolution finer than the accepted occupational exposure limit for the target gas. For gas sensors, the resolution has the same unit as gas concentration (ppm).

- Sensitivity [115].

Sensitivity represents the lowest measurable concentration of a gas sensor and is an absolute quantity. Sensitivity is the ability of a sensor to correctly measure the target gas.

- Operating temperature

Operating temperature indicates the ideal operating temperature range of a gas sensor and is usually united by degrees Celsius (°C). Sensors consist of electrical, chemical and optical elements. Hence, sensors must work in the demanded operating temperature range to obtain correct readings and good performances. Otherwise, sensors may operate abnormally and are exposed to permanent damages.

- Cross-sensitivity [116].

Cross sensitivity is a sensor's reaction to other gases which can "interfere" with how the sensor reacts. Exposing a sensor to a gas that is not the target gas can cause an undesirable effect; this may be a positive response, negative response or inhibition. Cross sensitivity is a non-dimensional number and is represented by a percentage.

- Stability

Stability of a sensor represents the degree that sensor characteristics keep constant over the lifetime. Variations of stability can be caused by components aging, components sensitivity reduction, signal to noise ratio change, etc.

- Durability

Durability is the ability of a sensor operating normally under proper functioning over its design lifetime without excessive repair requirement. In a real application, the durability of a sensor is represented by years of life, hours of use, and the number of operational cycles.

- Power consumption

Electric power is required by internal electronics of sensors to maintain normal working. Quantity of sensors are fitted on real vehicles; hence, sensors featuring low power consumptions provide advantages in practical applications.

- Cost & Maintenance

Cost is necessary to be considered in real applications. Sensors owning high performances are no doubt important for monitoring system state and performing control strategy timely. On the contrary, a compromise between sensor performance and cost is an inevitable part of commercialization. Furthermore, sensors which are easy for maintenance is also an important aspect in practical applications.

The main characteristics of different gas sensors are compared and presented in Fig. 4. Both advantages and disadvantages exist for different gas sensors [107]. Compared with other three types of gas sensors, the overall performances of electrochemical gas sensor and solid-state gas sensor are at relative high levels. However, the solid-state gas sensors have higher power consumption and are more prone to be affected by interference gases [107]. Hence, electrochemical gas sensors are more suitable for the environment system in FCEV application.

2.2.5. In-lab developed gas sensor

The developments of in-lab prototype gas sensors are compared in Table .5 and their operating principles are also detailed.

2.2.5.1. Optical fiber-based sensor. Optical fiber-based techniques are widely used in the new gas sensors. Hung et al. [118] developed a portable oxygen, carbon dioxide and ammonia detector based on optical fiber array. In the sensor array, Long-Period Fiber Grating (LPG) and FBG technique are utilized to detect ammonia. LPG is also known as the transmission fiber grating and its period ranges from tens to hundreds of micrometers [118]. Hung et al. integrated the FBG and the LPG together as a mixed type fiber grating to measure the temperature and the concentration of NH_3. The sensing principle is based on varied light intensity measurement. The FBG is designed as the sensing element and the LPG is used as the filter. The loss bands exist in the transmission spectrum of LPG. Benefiting from the loss bands, a linear spectrum region is created with a wide range. The central reflection wavelength of FBG arranges particularly on this loss bands. When a variation of strain or temperature occurring, the central reflection wavelength of FBG shifts. The relative shift between the central reflection wavelength of FBG and the transmission spectrum loss bands of LPG leads to the reflected light intensity which is measured by the photodiode. The NH_3

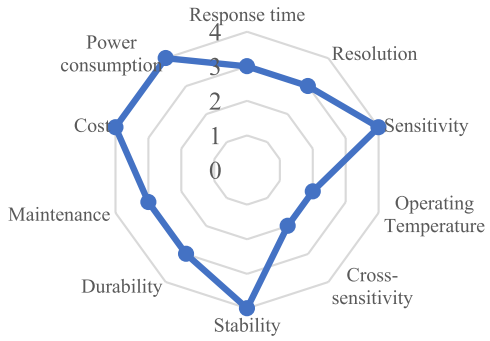

(a). Electrochemical sensor

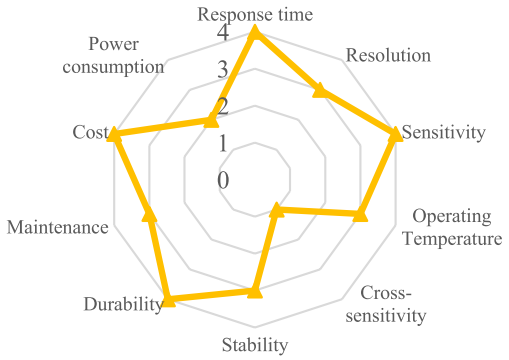

(b). Solid-State sensor

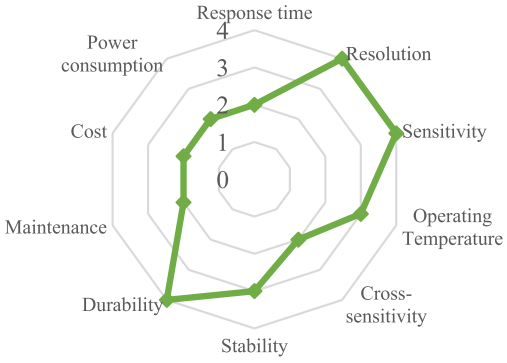

(c). NDIR sensor

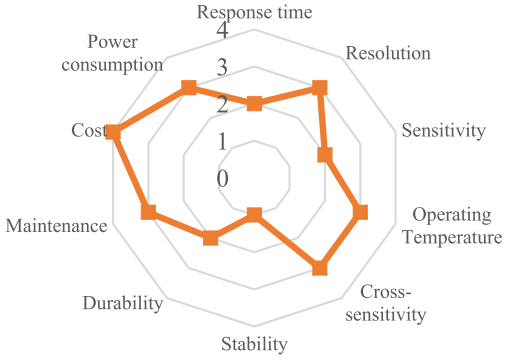

(d). Catalytic combustion sensor

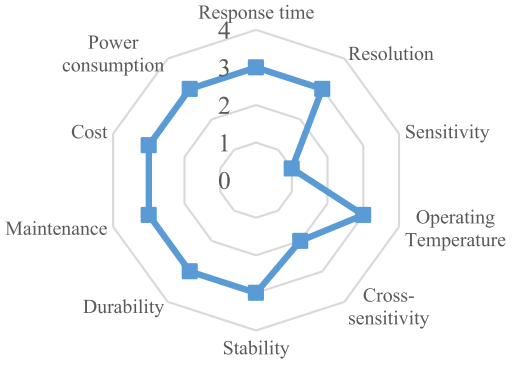

(e). Thermal conductivity sensor

Fig. 4. Characteristics comparison of various types of gas sensors (4: excellent; 3: good; 2: poor; 1: bad.).

sensing film is processed specially by the solution adjusting its pH value. Different concentrations of NH_3 changes reaction pH values of the sensing film to produce different wavelengths. Hence, the concentration of NH_3 can be measured.

Shao et al. [119] proposed a hydrogen sensor based on a single mode-no core-single mode (SNS) fiber interferometer structure. Pd/WO_3 film is used to coat the surface of the no core fiber (NCF) to measure the variation of hydrogen concentration. When the hydrogen concentration changes, the reflective index of NCF is changed, causing a shift into the resonant wavelength of the interferometer. Hence, the hydrogen concentration can be determined by measuring the shift of the resonant wavelength.

Nugroho et al. [120] firstly fabricate a noble metal (PdAu) alloy nanostructure arrays by Hole-Mask Colloidal Lithography (HCL). Then,

Table 5
Gas sensor in-lab prototype development.

Technique		Sensible gas quantity	Tested Gas
Optical fiber [121]	FBG-based	Single	NH_3 [118]
	SNS fiber interferometer	Single	H_2 [119]
	Nano-plasmonic-based	Single	H_2 [120]
MEMS based	Catalytic combustion	Single	H_2 [110]
	–	Single	H_2 [122]
	NDIR (MEMS infrared emitter)	Single	CO_2 [124]
	Electrochemical	Two-in-one	NO, H_2S [14]
	Metal-Oxide	Two-in-one	NO_2, NH_3 [125]
	Ceramic MEMS micro-heater	All gases	CO, H_2 [123]
Carbon Nanotube gas sensor [126]	Electrothermal effect based	No information.	
Micro/Nano gas sensor	Micro-Hot-Platform (MHP) and Nanopore Array (NPA)	Reducing gas (H_2, CO, C_2H_5OH)	Ethanol [127]

the authors transfer the PdAu alloy nano-disk arrays onto optical fibers. In this way, a hysteresis-free optical fiber nano-plasmonic hydrogen sensor is produced. The nanoparticles of the optical fiber sensor adsorb hydrogen. Then, the evanescent field of the light transferred through the optical fiber varied by coupling to the localized surface plasmon resonance (LSPR) in the nanoparticles. The permittivity of the nanoparticles is proportional to the hydrogen concentration in the optical fiber environment. The transmitted light intensity is rose which has a wavelength-dependent variation. Then, the light is reflected back by an aluminum mirror at the tip into a spectrometer through a bypass fiber. The produced optical fiber hydrogen sensor owns a significantly shorter response time and excellent stability to increasing and decreasing hydrogen partial pressure in the optical fiber sensors' environment.

2.2.5.2. MEMS-based sensor. Solid-state gas sensor requires heat-plate to heat the sense element up to the operating temperature. MEMS technique is usually utilized to minimize the volume of heat-plate. Micro-heaters based on MEMS technique can be much tinier than the conventional heat-plate ones. The operating temperature can increase much faster while the stability and durability are also improved.

Lee et al. [110] proposed a catalytic combustion hydrogen sensor which is fabricated by MEMS technology. The basic operating principle of the proposed sensor is the same as the traditional catalytic combustion gas sensors. The innovation point of this work is that the sensing elements and the reference elements are integrated into the suspended micro heaters, respectively. The micro heaters are fabricated by MEMS technology owning several advantages such as low power consumption, small size, fast response and quick recovery.

Gerdroodbary et al. [122] made a numerical study of a micro electrochemical In-plane Knudsen Radiometric Actuator (MIKRA) for hydrogen detection. MIKRA operates based on the thermal-driven force inside the MEMS sensor. Two micro beam arrays are separated on the plate of MIKRA by a small gap on the order of microns. One micro array is moveable, and the other is fixed. Hydrogen flow inside the sensor can make the moveable array move towards or backwards the fixed micro array. The motions are measured via a series of comb sense capacitors. Depending on the numerical study, the performance of MIKRA is affected by hydrogen concentration, temperature and partial pressure.

Vasiliev et al. [123] developed ceramic MEMS platforms for chemical sensors to assure micro-hotplate stable at high temperature. The range of working temperature was increased to 550 °C at least. CO and hydrogen mixture gas test were conducted as an example. The sensor was heated up to 450 °C and the concentrations of CO and hydrogen were both 3 ppm. The selectivity coefficient (CO to hydrogen) reached up to 10 and the power consumption reduced down to 50 mW. Prajesh et al. [125] proposed a two-in-one metal-oxide gas sensor (NO_2 and NH_3) integrated with micro-heater using MEMS techniques. The sensor operating temperature increased to 343 °C with power consumption lower than 86 mW. Although significant fast responses were achieved, the proposed sensor was only validated by NO_2 of 200 ppm and NH_3 of 5000 ppm which were under high concentration conditions.

MEMS technique is also considered in NDIR gas sensor. Vincent et al. [124] also developed a novel NDIR CO_2 sensor which was based on MEMS silicon on insulator (SOI) wideband infrared (IR) emitter for breath analysis. The novelty of this study is that MEMS silicon on insulator wideband infrared emitter is employed. The proposed NDIR sensor obtains the features like low power consumption, fast response, low concentration detectable, etc. The detectable concentration of CO_2 was up to 50 ppm with an 80 mm path length bench top detection system while the power consumption was reduced down to 0.35W.

Gatty et al. [14] proposed a two-in-one electrochemical sensor measuring the nitric oxide (NO) gas and the hydrogen sulphide (H_2S) gas for asthma monitoring. The basic operating principle is similar to the tradition electrochemical gas sensor. The innovation of this work is that the working electrode of the proposed sensor is fabricated by MEMS process. The proposed senor has the parts-per-billion (ppb) detection capability and features fast response characteristic.

Prajesh et al. [125] presented the design, fabrication and characterization of a two-in-one metal-oxide gas sensor detecting the nitrogen dioxide (NO_2) gas and the ammonia (NH_3) in industrial applications. The authors utilize MEMS technology to fabricate a platinum micro-heater integrating inside the proposed metal-oxide gas sensor. Therefore, the power consumption of the proposed sensor is low and the response is fast for both NO_2 and NH_3 measurements.

2.2.5.3. Other techniques-based sensor. There are also other novel technique-based gas sensors, for example, the carbon nanotube-based gas sensor [126] and the micro/nano gas sensor [127] which were for gas detection.

Kawano et al. [126] proposed a gas sensor which is based on the electrothermal effect of a multiwalled carbon nanotube (MWCNT) and has the capabilities of sensing both gas pressure and species. When the tested gas mixture occurs in the sensor, the conductive heat-transfer variations of gas molecules result in the change of the resistance of a heated MWCNT. In order to realize this mechanism, a suspended MWCNT is constructed between two Si Microstructures: the hot growth structure and the cold second structure. By the local electrical-field-guided chemical vapor deposition, the hot growth structure activates the MWCNT growth and the cold second structure provides bias of the local electrical field. The proposed MWCNT electrothermal sensors feature compact structure, fast and reversible in responses, and capability of integrating with microelectronics.

Xu et al. [127] proposed a new strategy towards the in-situ wafer-level fabrication of SnO_2 nanopore array (NPA) gas sensing chip integrated with micro-hot-platform (MHP). Solid-state gas sensors widely employ tin dioxide (SnO_2) since it has high sensitivity, low operating temperature and low cost. When SnO_2 is exposed to a reducing gas, for example, hydrogen, electrons are released back to SnO_2 due to surface reactions. Then, the resistance of the space charge layer is decreased. The proposed solid-state sensor gains features like high sensitivity (down to ~20 ppb), fast response time (down to ~1s) and low power consumption (down to ~30 mW to reach up to 350 °C).

In summary of the new technique-based gas sensors, the miniaturization is an obvious trend. Meanwhile, high accuracy, fast response, high stability and high durability are also required. Moreover, the power consumption of sensor must be reduced. Gas sensor which can avoid the cross sensitivity to un-target gas is undoubtedly attractive. Similar to the development of physical sensors, all-in-one gas sensors which have good selectivity are also welcomed.

2.3. Sensor selection process

2.3.1. Sensor selection

Development of sensor technologies contributes to improving sensor performances in various applications. In addition, the sensor selection process is also becoming more complex due to the progress. Sensors based on different technologies are designed for different applications. Hence, during the sensor selection process, once the target property and the application are confirmed, the first step is to select a sensor type which is suitable for the specific purpose. For example, both the capacitive humidity sensor and resistive humidity sensor can measure the relative humidity of gas stream in a fuel cell stack. Nevertheless, the performance of a resistive humidity sensor can be affected by temperature fluctuation of gas stream while the capacitive humidity sensor can work stably. Thus, the capacitive humidity sensor is the suitable type of sensor for relative humidity measurement in fuel cell applications.

In Fig. 5, a diagram is presented to illustrate the selection processes of physical sensors and gas sensors. The sensor selection is a process of making compromise among the characteristics of candidates. To be emphasized, the comparisons of gas sensor characteristics are not limited among the typical specifications, e.g., response time, resolution, measurement range, operating temperature, price, etc. The cross-sensitivity of gas sensor also must be taken into consideration. The output signal of gas sensor can be influenced significantly if high-level cross-sensitivity exists. The gas sensor cross-sensitivity can be compared from two aspects: firstly, the quantity of possible cross-sensitive gases, which is mainly depending on the natures of cross-sensitive gases; secondly, the effect degree of each possible cross-sensitive gas. Obviously, a gas sensor, which features fewer cross-sensitive gases and harder to be affected, is more suitable for the environment sensor system in real FCEV applications.

2.3.2. Sensor position in PEMFC system

According to the literature, a typical PEMFC system is illustrated as Fig. 6. The fuel cell stack is integrated with other four auxiliary parts: hydrogen supply sub-system, air supply sub-system, temperature management sub-system and environment sensor system.

The hydrogen supply sub-system maintains the hydrogen supply of the stack. At the outlet of the hydrogen tank, a pressure sensor is fitted to monitor the tank pressure. The hydrogen enters the stack from the anode inlet and is recycled at the anode outlet. The pressure sensor, mass flow meter and temperature sensor are installed at the inlet of anode while the pressure sensor, temperature sensor and relative humidity sensor are located at the outlet of anode. At the hydrogen inlet, the pressure is

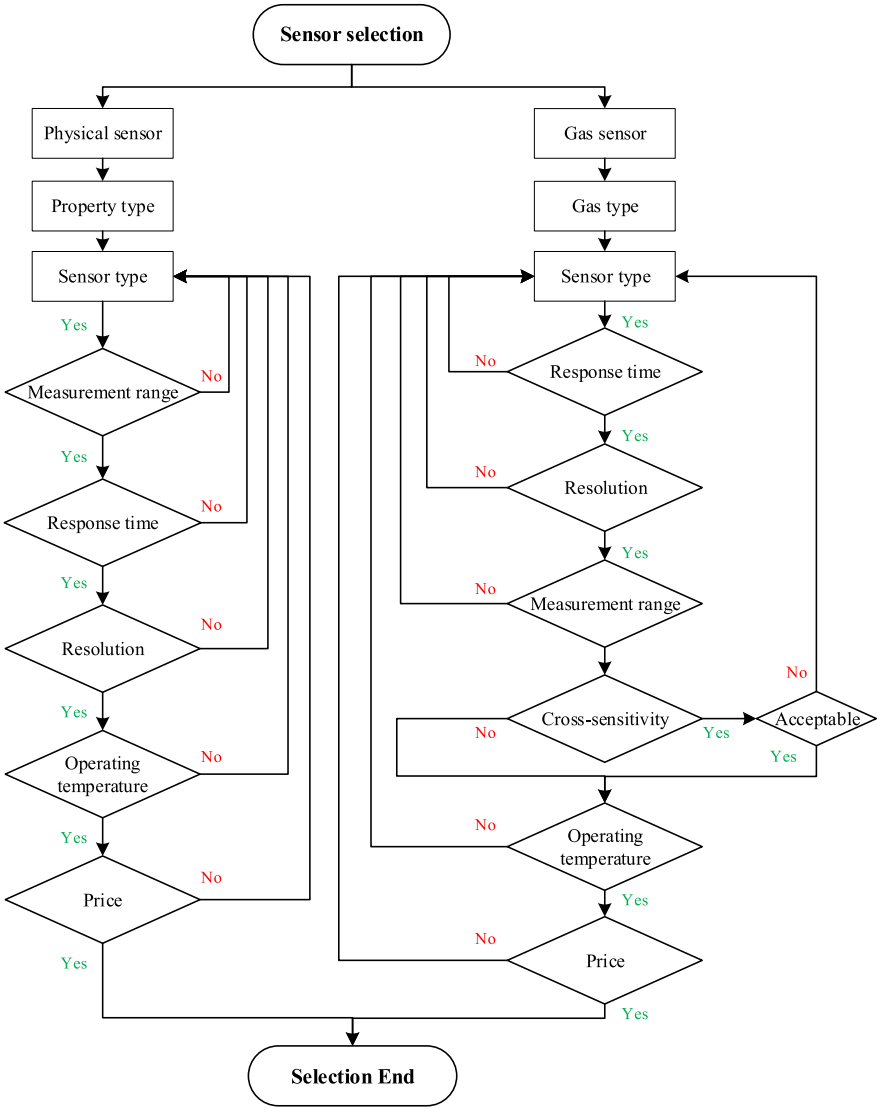

Fig. 5. Diagram of sensor selection process.

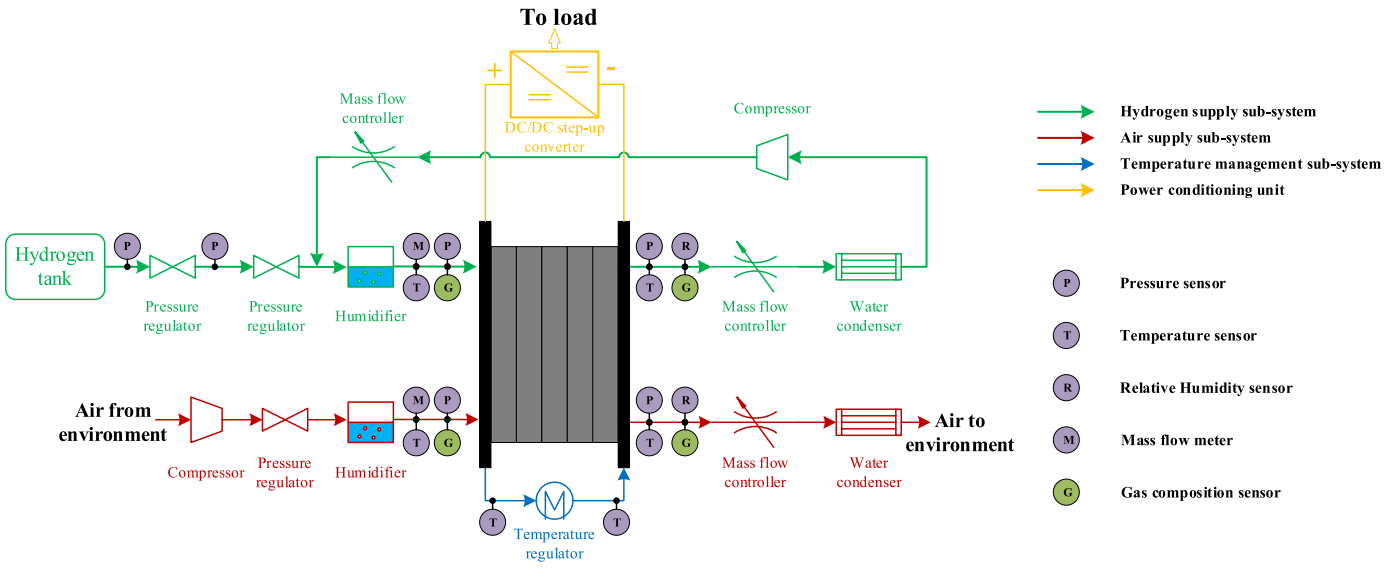

Fig. 6. Illustration of sensor position in PEMFC system [5,88,128,129].

measured by the pressure sensor. Hydrogen intake flow rate is measured by the mass flow meter. Thanks to the upstream humidifier for hydrogen, hygrometry level of reactant gases can be regulated and monitored by the relative humidity sensor at the hydrogen inlet. At the hydrogen outlet, the downstream gases pressure, temperature and relative humidity are also measured by the sensors respectively to monitor the operating state of the stack.

At the cathode, the installation of the sensors in the air supply sub-system is the same as in the hydrogen supply sub-system. Hence, the mass flow rate of hydrogen fuel and air can be well detected and controlled. Furthermore, the stack humidity can also be monitored. In the air supply subsystem, air flow rate and air pressure in the stack are regulated by the downstream mass flow controller. The air inlet flow rate and inlet pressure can be measured by the mass flow meter and pressure sensor separately. Similarly, hygrometry level of intake air is regulated by the upstream humidifier and monitored by the relative humidity sensor at the air inlet. At the air outlet, the downstream air pressure, temperature and relative humidity sensors are also installed to monitor the operating condition inside the cathode channels.

The main element of the temperature management sub-system is the temperature regulator. The liquid temperature sensors are installed at both inlet and outlet of the regulator. Therefore, the flow rate of coolant can be well-controlled to maintain the stack temperature in the optimal range.

The environment sensor system, which consists of gas sensors, is installed at the inlet and outlet of anode and cathode respectively to detect the possible gas contaminations and to analyze their impact of PEMFC.

2.3.3. *Fuel cell internal temperature measurement*

To be emphasized, non-negligible temperature differences exist inside fuel cells, which can be caused by different membrane materials, different gas diffusion layer materials as well as different gas flow channel structures of a bipolar plate. In many studies [5,88,128,129], fuel cell stack temperatures are represented by coolant temperatures which are measured by the temperature management sub-system. However, complex electrochemical reactions inside a fuel cell stack result in the cell temperatures differing from each other at various locations. Moreover, the non-uniform internal temperature distributions lead to internal water distribution differences. Hence, it is necessary to study the internal temperature distributions of a fuel cell stack no matter for performing water-management or for modeling fuel cell reactions more precisely. Temperature sensors, which are essential equipment for temperature measurements, attract main research attentions to study internal temperature distributions of fuel cell stacks. To realize this objective, the following characteristics are requested to be satisfied:

- sensors are embeddable inside fuel cells;
- sensors feature fast response, good sensitivity, stability, etc.;
- appropriate locations must be selected to integrate sensors in fuel cells;
- embedded sensors don't affect normal fuel cell stack performances;
- embedded sensors own certain mechanical strength.

It is evident that sensors are required having a small size to be embedded inside fuel cells measuring temperatures at different locations, e.g., the temperature in center of a fuel cell [64].

Shao et al. [61] punched on the opposite side of the air flow field of the cathode plate and installed twenty-seven commercial sensors by through holes. The sensors are distributed into five channels and in each channel, the spaces between sensors are uniformed to measure the temperature variation in the airflow direction. On the one hand, although the temperature distributions are precisely measured, the through-holes must be well sealed to avoid leakage of air. On the other hand, the proposed method is less suitable for a fuel cell stack since the temperatures of interlayers can't be measured by it. The FBG-based temperature sensors [59] and the micro-thermocouples [63] have also been provided to study internal temperature distributions of a fuel cell. However, the main drawback of these two means is that grooves are requested to be processed on the ribs separating the flow channels of the cathode flow plate to land the sensors.

The flexible MEMS-based micro temperature sensors [62,64–67] ant the thin film thermocouples [50,69] are the most attractive methods to measure the internal temperature distributions of a fuel cell or a fuel cell stack. The sensors have the abilities as good sensitivity, fast response, small and flexible size, good mechanical strength, etc. The product thickness of these two types of sensors is tens of micrometers, and the sensors are possible to be located at anywhere inside fuel cell without affecting its normal performances. Furthermore, the bipolar plate can be integrated with the sensors without any special processing.

Different measurement locations inside a fuel cell influence monitoring result a lot. Meanwhile, different gas flow channel structures of bipolar plates affect the measurement points selection. Serpentine flow channel and parallel flow channel are mostly used according to the studies [59,61,66,67]. For bipolar plate which is based on parallel flow channels, it can be classified as the inlet area, the center area and the

outlet area as in Fig. 7(a) [59,61–63,69]. At each area, two sensors can be located at both sides of the cell separately. Moreover, another sensor can also be embedded at center of the cell where the highest temperature appears [64]. For bipolar plate based on serpentine flow channels, temperature sensors can be embedded at turnings, center, as well as gas inlet and outlet ports as in Fig. 7(b) [50,65–67]. In this way, internal temperature distribution of a fuel cell can be completely measured for in-situ monitoring.

3. Investigation of PEMFC sensor selection techniques

PEMFC sensor selection techniques consist of two closely related parts: sensor-set size optimization and optimized sensor-set validation. Sensor-set size optimization focuses on selecting a minimal set of sensors to maintain PEMFC system operating normally. Naturally, it is essential to validate whether the optimized sensor-set can keep even diagnose and predict system performance or not. During optimization, selection of proper evaluate indexes is the key issue to be settled. On the other hand, utilization of appropriate diagnosis and/or prediction algorithms is important in term of optimized sensor-set validation.

In section 3, correlative literatures of these two parts are reviewed separately. A framework is proposed at the end of this section to illustrate PEMFC sensor selection techniques.

3.1. Sensor-set size optimization approaches

Although sensors are essential in FCEVs, high quantity of sensors can not only lead to the increase of system complexity but also make the cost and weight increase. Therefore, sensor-set size is meaningful to be optimized. Sensor-set size optimization approaches are reviewed in Table .6. The key technology concept of sensor-set optimization is to extract the most important features.

In PEMFC systems for FCEV, sensors are used for several purposes: system control, stack performance monitoring and PHM. However, too many signals can lead to an increase of calculation amount and meanwhile an increase in the complexity of the algorithm. Even worse, the interference of signal features will reduce the accuracy and efficiency of the PHM of the stack [16].

Hence, the purpose of sensor-set size optimization for PEMFC system is to reduce the sensor-set size as much as possible while guaranteeing the system normal performance and improving the efficiency and accuracy of PHM.

The optimization approaches can be classified into model-based ones, data-driven ones and hybrid ones.

The model-based approaches require a good understanding of the system and it is really difficult to model the system with very high accuracy. With respect to PEMFC applications, Sarrate et al. [132] reviewed three different model-based methods to optimize sensor placement for fault detection and isolation (FDI) purpose. 8 candidate sensors were used and the heuristic approach was the most efficient as the solution was found in 0.12 s. The two optimal sensors were cathode and anode pressure sensors. In Ref. [132], cost of sensor was the optimizing index and was assigned according to the ease of installation and the price of corresponding sensor.

Towards the data-driven approaches, huge amount of data-sets are requested. Data-driven approaches are always based on statistical methods, signal processing methods and artificial intelligence methods [133]. Lin et al. [136] applied Incremental Principle Component

Table 6
Sensor-set size optimization approach.

Ref.	Application field	Approach	Type	Original sensor-set size	Optimized sensor-set size
[132]	PEMFC system	Incremental search; Heuristic search; BILP	Model-based	8	2 (cathode pressure; anode pressure)
[16]	PEMFC system	Sensor sensitivity & noise resistance-based	Hybrid	16	3 (stack temperature; cathode outlet flow; cathode inlet flow)
[134]	PEMFC system	Sensor sensitivity & noise resistance-based	Hybrid	10	3 (stack temperature; cathode outlet flow; cathode inlet flow)
[17]	PEMFC system	Sensor sensitivity & Stack failure mode weighting based	Hybrid	10	4 (cathode inlet flow; cathode outlet flow; anode outlet flow; stack temperature)
[135]	PEMFC system	Sensor sensitivity & noise resistance-based	Hybrid	9	No information.
[136]	PEMFC system	PCA method	Data-driven	20	8
[19]	SOFC system gas supply unit	PCA method	Hybrid	–	–
[18]	PEMFC system	WPT	Data-driven	9	4 (stack thermocouple; cathode outlet thermocouple; cathode outlet pressure gauge; anode outlet humidification sensor)

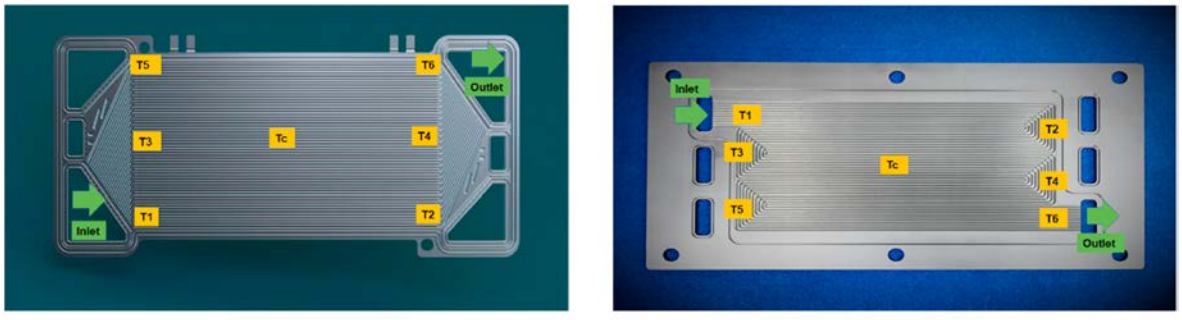

(a) [130] (b) [131]

Fig. 7. Embedded temperature sensors locations on bipolar plate based on (a) parallel flow channels [130] (b) serpentine flow channels [131].

Analysis (IPCA) algorithm to generate proper features for PEMFC diagnosis. IPCA algorithm was compared with other two methods: Factor Analysis (FA) and Linear Discriminant Analysis (LDA). Compared with FA algorithm, IPCA calculation was much time-saving. On the other hand, LDA reduced the data dimension too much and loose effective information. The original sensor-set size was 20 and reduced to 8 by IPCA. Mao et al. [18] used wavelet packet transform (WPT) to extract sensor features, evaluate sensor conditions and reduce sensor-set dimension. Finally, the original sensor-set with 9 sensors was decreased to 4 sensors. The optimal sensors were used for PEMFC diagnosis and abnormal sensor identification.

Hybrid approaches are also developed for PEMFC performance prediction. Mao et al. [16,134,135] proposed a sensor sensitivity and noise resistance-based method to optimize sensor-set size of PEMFC system. Sensor sensitivities were generated based on the numerical fuel cell model and were defined as the percentage variation in sensors due to the unit change in fuel cell health parameters. Membrane resistance, cell active area and liquid water inside cell were chosen as the health parameters. Sensor measurement noise was also used in the selection process and was expressed by a set of response errors which were generated randomly in the range of ± 2% sensor measurements. Sensor-set sizes were reduced from 16 to 3 and from 10 to 3 in Refs. [16, 134] respectively. In Ref. [17], Mao et al. proposed the sensor sensitivity and stack failure mode weighting-based optimization method. The sensor sensitivity generation was the same as in Refs. [16,134,135]; three failure modes (flooding, membrane dehydration and cell active area reduction) of the fuel cell were selected which caused various levels of system performance degradation. The original sensor-set size was reduced from 10 to 4. Meanwhile, compared with sensor sensitivity and noise resistance-based approach, the proposed method in Ref. [17] was time-saving.

In summary, hybrid optimization approaches own more advantages than model-based and data-driven methods. During the design of optimization algorithm, the effectiveness differs a lot among various methods. The algorithms which owns short calculation period are more attractive. Meanwhile, different evaluate items can lead to different optimization results. Thus, it is essential to select proper evaluation indexes to make a good selection among the sensors.

3.2. Optimal sensor-set validation approaches

A complete sensor-set size optimization procedure must contain the validation process of the selected sensors. The purpose of validation is to verify the correctness, effectiveness and accuracy of the system only based on the optimal sensor-set. Various validation approaches are reviewed in Table .7.

Table 7
Optimal sensor set validation approaches.

Ref.	Approach	Type	Algorithm	Fault type	On/ Off-line
[16]	Performance prediction	Data-driven	ANFIS	–	Off-line
[134]	Performance prediction	Data-driven	ANFIS	–	Off-line
	Fault diagnosis		KPCA, WPT, SVD	Flooding	
[17]	Fault diagnosis	Data-driven	KPCA, WPT, SVD	Flooding	On-line
[135]	Fault diagnosis	Data-driven	WPT, KPCA	Flooding; Dehydration	On-line
[136]	Fault diagnosis	Data-driven	Random forest algorithm	No information	Off-line
[19]	Fault diagnosis	Data-driven	PCA; EWMA control chart	–	Off-line & On-line
[18]	Fault diagnosis	Data-driven	KPCA, WPT, SVD	Flooding	On-line

The performance prediction of fuel cell is the most direct method. Mao et al. [16] proposed ANFIS approach to validate the capability of selected sensor-set by using the PEMFC test data from IEEE 2014 PHM data challenge [137]. Two constant current loading conditions were selected: a constant current of 0.7 A/cm^2, and a constant current of 0.7 A/cm^2 with high frequency (5 kHz) current ripples (±10% of the constant value). The authors indicated that the performance predictions of fuel cell stack voltages were with good qualities.

Fault diagnostics are mostly utilized to validate the optimal sensor-set for PEMFC system. Mao et al. proposed off-line and on-line PEMFC fault diagnostics to validate optimal-sensor set in literatures [17,134] respectively. Fuel cell flooding faults, which were tested based on an 80W fuel cell stack of Pragma Industries, were selected for the diagnosis. The proposed approach used Kernel Principal Component Analysis (KPCA) to reduce the dataset dimension, Wavelet Packet Transform (WPT) to extract features and Singular Value Decomposition (SVD) to determine the features containing most useful information for the classification. According to the results, the flooding faults were distinguished clearly as normal state, transition state and flooding state by using the selected sensors. No confusion existed among the three states by the comparison between predicted results and actual datasets. Mao et al. [135] also validated the capability of optimal sensor-set by using flooding fault and membrane dehydration fault together. With the selected sensors, both normal state and faulty state were clearly separated. Furthermore, the flooding state and dehydration state were also distinguished obviously. In Ref. [18], authors verified the performance of selected sensors also by the fuel cell flooding faults which were classified as normal state, minor flooding state, medium flooding state and severe flooding state. The improvement in Ref. [18] was that based on the optimal sensor-set, the four fault states were discriminated clearly and no confusion existed. The results indicated that with the proposed technique, the fuel cell faults could be identified at early stage. Lin et al. [136] used various data-driven approaches to validate the selected sensors. Compared with classifiers as Support Vector Machine (SVM), K-Nearest Neighbors (KNN) algorithm, Artificial Neural Network (ANN) algorithm, decision tree and Boosting algorithm, Random Forest (RF) classifier obtained the best average results with the experiment datasets of selected sensors.

Therefore, among different approaches, data-driven methods are favored due to that the validation results can be evaluated comparatively with real tested datasets, and in practical fuel cell systems, accurate physical models are extremely difficult or even impossible to be developed [138]. Machine learning methods are already widely used in PEMFC developments such as performance prediction, material selection and PHM [143]. The algorithms such as Grid Long-Short-Term Memory (G-LSTM) cell based Recurrent Neural Network (RNN) [139], Echo State Networks (ESN) [140,141], Gray Neural Network Model (GNNM) [142] and Greedy-NAR (Nonlinear Autoregression) [144] are also attractive to be employed for sensor-set size optimization and optimized sensor validation.

3.3. Sensor-set optimization and validation framework

To summarize the comparative studies done in section 3.1 and 3.2, a framework which explains sensor-set optimization and validation step by step is proposed as illustrated in Fig. 8.

In sensor-set size optimization process, firstly, the optimizing index is essential to be defined. According to the literatures review, sensor sensitivity and sensor noise-resistance are proven to be effective indexes. Then, the optimization approach type and proper algorithm can be selected. The hybrid algorithms are promising solutions which combine the advantages of model-based methods and data-driven methods. Once the optimized sensor-set size and time consumption are acceptable, the optimal sensor-set candidates can be confirmed.

At the beginning of validation step, the approach type and validation

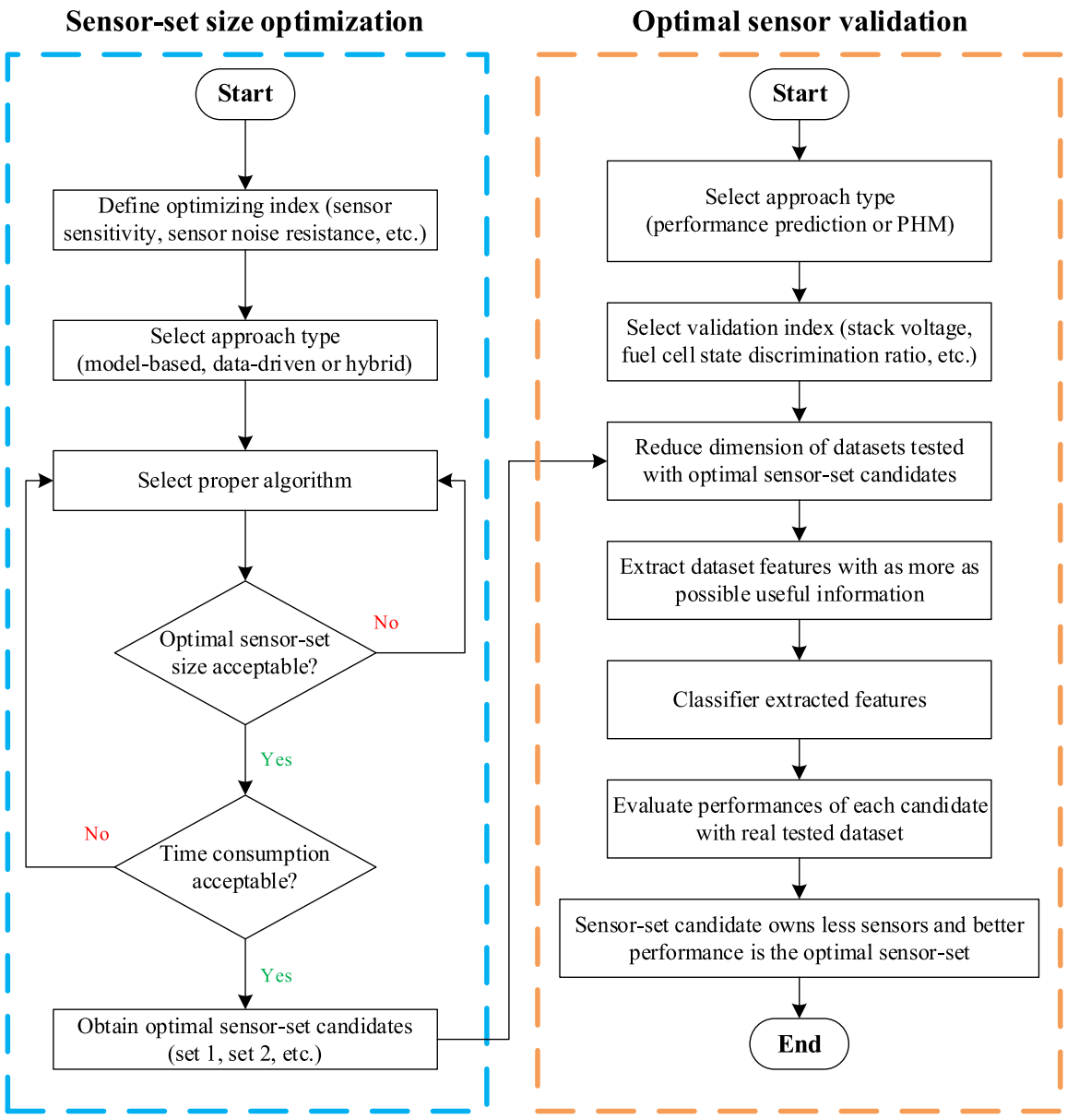

Fig. 8. Diagram of sensor-set optimization and validation procedure.

index are necessary to be determined. PHM of PEMFC system is usually utilized to verify the performance of sensor-set candidate. For the purpose of improving algorithm time consumption, the dimensions of dataset tested by sensor-set candidates are requested to be reduced. Before validating the performances of sensor candidates, dataset features with as more as possible useful information will be extracted and classified. Finally, sensor-set which feature smallest size and best performance is determined as the optimal solution.

4. Conclusion

In this paper, the sensor-set developments and optimization approaches for the PEMFC system in FCEV applications are reviewed.

The sensors are classified as physical sensors and gas sensors. Physical sensors are used to detect the essential physical signals, e.g., hydrogen mass flow rate, liquid coolant temperature, air pressure, stack relative humidity, etc. The physical sensors are necessary for the system control, stack state detection and performance monitoring. A comparative analysis of physical sensor development has been done in this study.

The gas sensors consist of the hydrogen leakage detectors and the environment sensor system. The hydrogen leakage detectors are essential to be fitted on the actual FCEV for the safety reason as hydrogen belongs to combustible gases. Meanwhile, since gas contaminations can lead to fuel cell performance degradations and even irreversible damages to the stacks, the environment sensor system is promising to be integrated with PEMFC systems to reduce gas impurities impact on the stack. Both commercialized sensors and in-lab prototype sensors are reviewed in order to generally analyze the current status and research trend of sensors used in the design of PEMFC systems for FCEV application. Electrochemical sensors are most suitable for the detection of gas contaminations. Sensors with MEMS technique gain advantages such as miniaturization, low power consumption, fast response, high accuracy, etc. Then the sensor selection process of both physical sensors and gas sensors has been proposed in this study.

Although more sensors can help obtain more information, the cost and complexity of PEMFC system will also be increased. Hence, the sensor-set size is required to be optimized to realize the most effective

fault diagnosis, remaining useful estimation and health-monitoring of the PEMFC system. The sensor-set size optimization approaches for the fuel cell system applications have been reviewed. Meanwhile, the optimal sensor-set validation methods have also been concluded. The hybrid approaches are mostly used for the optimization purpose while the data-driven methods are widely used for the validation. Finally, a framework of sensor-set optimization and validation is proposed.

Finally, following perspectives are given according to this study.

- Physical sensors: For FCEV applications, integrated and miniaturized physical sensors are more suitable to reduce the complexity of a PEMFC system. Operating principles of various physical sensors, which are reviewed and compared in this study, also provide the possibility of realizing this purpose. For example, relative humidity measured by a capacitive humidity sensor is a function of both the ambient temperature and water vapor pressure. Thermal mass flow meters are based on the variation of heat carried by gas flow stream. Hence, an integrated temperature, pressure, relative humidity and mass flow sensor is possible to be fabricated. Meanwhile, flexible micro-sensor based on MEMS technology provides the ability to miniaturize sensors even embedding inside a fuel cell without affecting the performance.
- Gas sensors: No matter for hydrogen leakage detector or environment sensor system, the ability of fast response is very important. Meanwhile, gas sensors are needed to be developed with a wider operating temperature range to satisfy different working conditions. Cost of gas sensors is also required to be reduced. Moreover, the environment sensor system is supposed to have better selectivity of a gas mixture, and own fewer cross-sensitivity to non-targeted gases.
- Sensor-set size: For sensor-set size optimization, proper evaluation indexes and optimization algorithms must be selected or proposed. Hybrid method and data-driven method are mostly used during optimization. Machine learning algorithms which show advantages in PHM of PEMFC are promising to be utilized for sensor set-size optimization and optimized sensor set validation. However, the majority of fuel cell operating conditions are tested under steady states. Hence, fuel cell state is needed to be measured with dynamic processes and even based on real driving profiles. Only in this way, an optimized sensor set can be suitable for real FCEV applications. For validation of optimized sensor-set size, more types of PEMFC faults are needed to be taken into consideration, e.g., carbon monoxide poisoning, catalyst degradation, starvation, etc., to validate the performance of optimized sensor set more comprehensively.

Declaration of competing interest

The authors declare that they have no known competing financial interests or personal relationships that could have appeared to influence the work reported in this paper.

Acknowledgement

This work has been supported by the EIPHI Graduate School (contract ANR-17- EURE-0002) and the Region Bourgogne Franche-Comté.

References

[1] D. Hissel, M.C. Pera, Diagnostic & health management of fuel cell systems: issues and solutions, Annu. Rev. Contr. 42 (2016) 201–211.
[2] L. Xu, C.D. Mueller, J. Li, M. Ouyang, Z. Hu, Multi-objective component sizing based on optimal energy management strategy of fuel cell electric vehicles, Appl. Energy 157 (2015) 664–674.
[3] H. Wang, A. Gaillard, D. Hissel, A review of DC/DC converter-based electrochemical impedance spectroscopy for fuel cell electric vehicles, Renew. Energy 141 (2019) 124–138, 2019.
[4] D. Candusso, A. De Bernardinis, M.C. Péra, F. Harel, X. François, D. Hissel, J. M. Kauffmann, Fuel cell operation under degraded working modes and study of diode by-pass circuit dedicated to multi-stack association, Energy Convers. Manag. 49 (4) (2008) 880–895.
[5] S.R. Higgins, J. Ewan, J. St-Pierre, G. Severa, K. Davies, K. Bethune, R. Rocheleau, Environmental sensor system for expanded capability of PEM fuel cell use in high air contaminant conditions, Int. J. Hydrogen Energy 43 (50) (2018) 22584–22594.
[6] H2 tools, https://h2tools.org/sites/default/files/HondaClarityFuelCellERG.pdf, 2020. (Accessed 10 May 2020).
[7] Nissha Co, Ltd. https://www.nissha.com/english/news/2014/12/12th_1.html, 2020. (Accessed 10 May 2020).
[8] T. Hübert, L. Boon-Brett, V. Palmisano, M.A. Bader, Developments in gas sensor technology for hydrogen safety, Int. J. Hydrogen Energy 39 (35) (2014) 20474–20483.
[9] F. Jing, M. Hou, W. Shi, J. Fu, H. Yu, P. Ming, B. Yi, The effect of ambient contamination on PEMFC performance, J. Power Sources 166 (1) (2007) 172–176.
[10] Y. Nagahara, S. Sugawara, K. Shinohara, The impact of air contaminants on PEMFC performance and durability, J. Power Sources 182 (2) (2008) 422–428.
[11] X. Cheng, Z. Shi, N. Glass, L. Zhang, J. Zhang, D. Song, J. Shen, A review of PEM hydrogen fuel cell contamination: impacts, mechanisms, and mitigation, J. Power Sources 165 (2) (2007) 739–756.
[12] GmbH, Flexim. https://www.flexim.com/en/products/permanent-flowmeters-gases/fluxus-g801, 2020. (Accessed 30 September 2020).
[13] Robert Bosch GmbH, K. Reif, K.H. Dietsche, Automotive Handbook, Robert Bosch GmbH, 2014.
[14] H.K. Gatty, MEMS-based Electrochemical Gas Sensors and Wafer-Level Methods, Doctoral dissertation, KTH Royal Institute of Technology, 2015.
[15] R. Moos, K. Sahner, M. Fleischer, U. Guth, N. Barsan, U. Weimar, Solid state gas sensor research in Germany–a status report, Sensors 9 (6) (2009) 4323–4365.
[16] L. Mao, L. Jackson, Selection of optimal sensors for predicting performance of polymer electrolyte membrane fuel cell, J. Power Sources 328 (2016) 151–160.
[17] L. Mao, L. Jackson, B. Davies, Effectiveness of a novel sensor selection algorithm in PEM fuel cell on-line diagnosis, IEEE Trans. Ind. Electron. 65 (9) (2018) 7301–7310.
[18] L. Mao, L. Jackson, W. Huang, Z. Li, B. Davies, Polymer electrolyte membrane fuel cell fault diagnosis and sensor abnormality identification using sensor selection method, J. Power Sources 447 (2020), 227394.
[19] X.L. Wu, Y.W. Xu, D.Q. Zhao, Z.H. Li, X.B. Zhong, M.T. Chen, X. Li, Fault detection and assessment for solid oxide fuel cell system gas supply unit based on novel principal component analysis, J. Power Sources 436 (2019), 226864.
[20] R. Khelif, B. Chebel-Morello, S. Malinowski, E. Laajili, F. Fnaiech, N. Zerhouni, Direct remaining useful life estimation based on support vector regression, IEEE Trans. Ind. Electron. 64 (3) (2016) 2276–2285.
[21] D. Hissel, R. Gouriveau, PHM of Fuel Cell Systems – a State of the Art, Tutorial, IEEE Industrial Electronics Conference, Vienna, Austria, 2013.
[22] Suzuki, T., & Tsutsui, M. U.S. Patent No. 4,829,814. Washington, DC: U.S. Patent and Trademark Office (1989).
[23] Stoltman, D. D., Kabasin, D. F., & Field, M. J. U.S. Patent No. 4,445,369. Washington, DC: U.S. Patent and Trademark Office (1984).
[24] M. Rittmann, R. Moritz, S. Bauer, U. Konzelmann, Air flow meter 8. Generation: a modular approach for new diesel system challenges, in: Advanced Microsystems for Automotive Applications, Springer, Heidelberg, 2013, pp. 363–371.
[25] S.O. Akansu, S. Tangöz, N. Kahraman, M.İ. İlhak, S. Açıkgöz, Experimental study of gasoline-ethanol-hydrogen blends combustion in an SI engine, Int. J. Hydrogen Energy 42 (40) (2017) 25781–25790.
[26] Mikulla, V. U.S. Patent No. 4,025,891. Washington, DC: U.S. Patent and Trademark Office (1977).
[27] Ueno, S., Sato, K., Oyama, Y., Nishimura, Y., & Miya, K. U.S. Patent No. 4,369,656. Washington, DC: U.S. Patent and Trademark Office (1983).
[28] Takahashi, M., Tokuda, H., Suzuki, T., Takada, M., & Kooriyama, T. U.S. Patent No. 4,790,182. Washington, DC: U.S. Patent and Trademark Office (1988).
[29] T. Gilles, Automotive Service: Inspection, Maintenance, Repair, Cengage Learning, 2012.
[30] Miyoshi, N., Tsuruoka, M., & Nagumo, M. U.S. Patent No. 4,584,883. Washington, DC: U.S. Patent and Trademark Office (1986).
[31] Sentronics, 2020. https://www.sentronics.com/products/flowsonic-hf/. (Accessed 10 May 2020).
[32] R. Bates, M. Battistin, S. Berry, J. Berthoud, A. Bitadze, P. Bonneau, E. Da Riva, A combined ultrasonic flow meter and binary vapour mixture analyzer for the ATLAS silicon tracker, J. Instrum. 8 (2) (2013). P02006.
[33] FTI Flow Technology. https://ftimeters.com/, 2020. (Accessed 10 May 2020).
[34] Zimmerman, D. J., & Dorman, F. D. U.S. Patent No. 5,325,728. Washington, DC: U.S. Patent and Trademark Office (1994).
[35] Morita, Y., Katayama, M., & Kato, T. U.S. Patent No. 4,648,281. Washington, DC: U.S. Patent and Trademark Office (1987).
[36] R.C. Baker, Turbine flowmeters: II. Theoretical and experimental published information, Flow Meas. Instrum. 4 (3) (1993) 123–144.
[37] Friese, K. H., Stecher, G., & Wiedenmann, H. M. U.S. Patent No. 5,142,266. Washington, DC: U.S. Patent and Trademark Office (1992).
[38] Amphenol Advanced Sensors. https://www.amphenol-sensors.com/en/thermometrics/assemblies/3439-a-1325, 2020. (Accessed 10 May 2020).
[39] Honeywell, 2020. https://sensing.honeywell.com/honeywell-sensing-temperature-sensors-line-guide-009033-4-en.pdf. (Accessed 10 May 2020).
[40] U. Kang, K.D. Wise, A high-speed capacitive humidity sensor with on-chip thermal reset, IEEE Trans. Electron. Dev. 47 (4) (2000) 702–710.

[41] P.J. Schubert, J.H. Nevin, A polyimide-based capacitive humidity sensor, IEEE Trans. Electron. Dev. 32 (7) (1985) 1220–1223.
[42] Y. Kim, B. Jung, H. Lee, H. Kim, K. Lee, H. Park, Capacitive humidity sensor design based on anodic aluminum oxide, Sensor. Actuator. B Chem. 141 (2) (2009) 441–446.
[43] D.U. Kim, M.S. Gong, Thick films of copper-titanate resistive humidity sensor, Sensor. Actuator. B Chem. 110 (2) (2005) 321–326.
[44] N.M. Kiasari, S. Soltanian, B. Gholamkhass, P. Servati, Room temperature ultra-sensitive resistive humidity sensor based on single zinc oxide nanowire, Sensor Actuator Phys. 182 (2012) 101–105.
[45] H. Farahani, R. Wagiran, M.N. Hamidon, Humidity sensors principle, mechanism, and fabrication technologies: a comprehensive review, Sensors 14 (5) (2014) 7881–7939.
[46] M.A. Najeeb, Z. Ahmad, R.A. Shakoor, Organic thin-film capacitive and resistive humidity sensors: a focus review, Advanced Materials Interfaces 5 (21) (2018), 1800969.
[47] Brooksinstrument, 2020. https://www.brooksinstrument.com/en/products/mass-flow-controllers/thermal-elastomer-sealed/sla5800-series. (Accessed 10 May 2020).
[48] Azbil Corporation. https://www.azbil.com/products/factory/download/catalog-spec/CP-PC-1333E-12.pdf, 2020. (Accessed 10 May 2020).
[49] K. Ikeda, H. Kuwayama, T. Kobayashi, T. Watanabe, T. Nishikawa, T. Yoshida, K. Harada, Silicon pressure sensor integrates resonant strain gauge on diaphragm, Sensor Actuator Phys. 21 (1–3) (1990) 146–150.
[50] S.T. Ali, J. Lebæk, L.P. Nielsen, C. Mathiasen, P. Møller, S.K. Kær, Thin film thermocouples for in situ membrane electrode assembly temperature measurements in a polybenzimidazole-based high temperature proton exchange membrane unit cell, J. Power Sources 195 (15) (2010) 4835–4841.
[51] J.M. LaManna, S.G. Kandlikar, Determination of effective water vapor diffusion coefficient in pemfc gas diffusion layers, Int. J. Hydrogen Energy 36 (8) (2011) 5021–5029.
[52] TE connectivity [Online]. Available, https://www.te.com/usa-en/product-CAT-HSA0004.html, 2020. (Accessed 27 May 2020).
[53] Honeywell, 2020. https://sensing.honeywell.com/HIH-4602-L-CP-humidity-sensors. (Accessed 10 May 2020).
[54] P. Paranthoen, C. Petit, J. Lecordier, The effect of the thermal prong—wire interaction on the response of a cold wire in gaseous flows (air, argon and helium), J. Fluid Mech. 124 (1982) 457–473.
[55] G. Pankanin, The vortex flowmeter: various methods of investigating phenomena, Meas. Sci. Technol. 16 (3) (2005) R1–R16.
[56] P. Schubert, J. Nevin, A polyimide-based capacitive humidity sensor, IEEE Trans. Electron. Dev. 32 (7) (1985) 1220–1223, 1985.
[57] Feyh, A., Graham, A., Samarao, A., Yama, G., & O'brien, G. U.S. Patent No. 9,588,073. Washington, DC: U.S. Patent and Trademark Office (2017).
[58] U. Demisch, U.S. Patent and Trademark Office, Washington, DC, 1991. U.S. Patent No. 5,050,434.
[59] N.A. David, P.M. Wild, J. Hu, N. Djilali, In-fibre Bragg grating sensors for distributed temperature measurement in a polymer electrolyte membrane fuel cell, J. Power Sources 192 (2) (2009) 376–380.
[60] N. David, K. Von Schilling, P.M. Wild, N. Djilali, In situ measurement of relative humidity in a PEM fuel cell using fibre Bragg grating sensors, Int. J. Hydrogen Energy 39 (31) (2014) 17638–17644.
[61] H. Shao, D. Qiu, L. Peng, P. Yi, X. Lai, In-situ measurement of temperature and humidity distribution in gas channels for commercial-size proton exchange membrane fuel cells, J. Power Sources 412 (2019) 717–724.
[62] C.Y. Lee, F.B. Weng, C.H. Cheng, H.R. Shiu, S.P. Jung, W.C. Chang, C.J. Lee, Use of flexible micro-temperature sensor to determine temperature in situ and to simulate a proton exchange membrane fuel cell, J. Power Sources 196 (1) (2011) 228–234.
[63] H. Pei, Z. Liu, H. Zhang, Y. Yu, Z. Tu, Z. Wan, W. Liu, In situ measurement of temperature distribution in proton exchange membrane fuel cell I a hydrogen–air stack, J. Power Sources 227 (2013) 72–79.
[64] C.Y. Lee, W.J. Hsieh, G.W. Wu, Embedded flexible micro-sensors in MEA for measuring temperature and humidity in a micro-fuel cell, J. Power Sources 181 (2) (2008) 237–243.
[65] C.Y. Lee, W.Y. Fan, C.P. Chang, A novel method for in-situ monitoring of local voltage, temperature and humidity distributions in fuel cells using flexible multi-functional micro sensors, Sensors 11 (2) (2011) 1418–1432.
[66] C.Y. Lee, F.B. Weng, Y.W. Kuo, C.H. Tsai, Y.T. Cheng, C.K. Cheng, J.T. Lin, In-situ measurement of high-temperature proton exchange membrane fuel cell stack using flexible five-in-one micro-sensor, Sensors 16 (10) (2016) 1731.
[67] H.Y. Wang, W.J. Yang, Y.B. Kim, Analyzing in-plane temperature distribution via a micro-temperature sensor in a unit polymer electrolyte membrane fuel cell, Appl. Energy 124 (2014) 148–155.
[68] S.T. Ali, J. Lebæk, L.P. Nielsen, C. Mathiasen, P. Møller, S.K. Kær, Thin film thermocouples for in situ membrane electrode assembly temperature measurements in a polybenzimidazole-based high temperature proton exchange membrane unit cell, J. Power Sources 195 (15) (2010) 4835–4841.
[69] Y.Q. Tang, W.Z. Fang, H. Lin, W.Q. Tao, Thin film thermocouple fabrication and its application for real-time temperature measurement inside PEMFC, Int. J. Heat Mass Tran. 141 (2019) 1152–1158.
[70] K.O. Hill, G. Meltz, Fiber Bragg grating technology fundamentals and overview, J. Lightwave Technol. 15 (8) (1997) 1263–1276.
[71] Y.J. Rao, Fiber Bragg grating sensors: principles and applications, in: K.T. V. Grattan, B.T. Meggitt (Eds.), Optoelectronics, Imaging and Sensing, Optical Fiber Sensor Technology, vol. 2, Springer, Boston, MA, 1998, pp. 355–379.
[72] J.J. Baschuk, X. Li, Carbon monoxide poisoning of proton exchange membrane fuel cells, Int. J. Energy Res. 25 (8) (2001) 695–713.
[73] Z. Qi, C. He, A. Kaufman, Effect of CO in the anode fuel on the performance of PEM fuel cell cathode, J. Power Sources 111 (2) (2002) 239–247.
[74] Z. Qi, C. He, A. Kaufman, Poisoning of proton exchange membrane fuel cell cathode by CO in the anode fuel, Electrochem. Solid State Lett. 4 (12) (2001) A204–A205.
[75] N. Rajalakshmi, T.T. Jayanth, K.S. Dhathathreyan, Effect of carbon dioxide and ammonia on polymer electrolyte membrane fuel cell stack performance, Fuel Cell. 3 (4) (2003) 177–180.
[76] R. Mohtadi, W.K. Lee, S. Cowan, J.W. Van Zee, M. Murthy, Effects of hydrogen sulfide on the performance of a PEMFC, Electrochem. Solid State Lett. 6 (12) (2003) A272–A274.
[77] M. Murthy, M. Esayian, W.K. Lee, J.W. Van Zee, The effect of temperature and pressure on the performance of a PEMFC exposed to transient CO concentrations, J. Electrochem. Soc. 150 (1) (2003) A29–A34.
[78] S. Knights, N. Jia, C. Chuy, J. Zhang, Fuel Cell Seminar 2005: Fuel Cell Progress. Challenges and Markets, California, Palm Springs, 2005.
[79] R. Mohtadi, W.K. Lee, J.W. Van Zee, Assessing durability of cathodes exposed to common air impurities, J. Power Sources 138 (1–2) (2004) 216–225.
[80] T. Loučka, Adsorption and oxidation of sulphur and of sulphur dioxide at the platinum electrode, J. Electroanal. Chem. Interfacial Electrochem. 31 (2) (1971) 319–332.
[81] A.Q. Contractor, H. Lal, The nature of species adsorbed on platinum from SO2 solutions, J. Electroanal. Chem. Interfacial Electrochem. 93 (2) (1978) 99–107.
[82] F.A. Uribe, S. Gottesfeld, T.A. Zawodzinski, Effect of ammonia as potential fuel impurity on proton exchange membrane fuel cell performance, J. Electrochem. Soc. 149 (3) (2002) A293–A296.
[83] R. Halseid, P.J. Vie, R. Tunold, Influence of ammonium on conductivity and water content of Nafion 117 membranes, J. Electrochem. Soc. 151 (3) (2004) A381–A388.
[84] A.L. Dicks, Hydrogen generation from natural gas for the fuel cell systems of tomorrow, J. Power Sources 61 (1–2) (1996) 113–124.
[85] C.N. Hamelinck, A.P. Faaij, Future prospects for production of methanol and hydrogen from biomass, J. Power Sources 111 (1) (2002) 1–22.
[86] J.H. Wee, K.Y. Lee, S.H. Kim, Sodium borohydride as the hydrogen supplier for proton exchange membrane fuel cell systems, Fuel Process. Technol. 87 (9) (2006) 811–819.
[87] S. Chugh, S. Meenakshi, K. Sonkar, A. Sharma, G.S. Kapur, S.S.V. Ramakumar, Performance evaluation of PEM fuel cell stack on hydrogen produced in the oil refinery, Int. J. Hydrogen Energy 45 (8) (2020) 5491–5500.
[88] S. Erbach, B. Pribyl, M. Klages, L. Spitthoff, K. Borah, S. Epple, T.J. Schmidt, Influence of operating conditions on permeation of CO2 through the membrane in an automotive PEMFC system, Int. J. Hydrogen Energy 44 (25) (2019) 12760–12771.
[89] A. Talke, U. Misz, G. Konrad, A. Heinzel, D. Klemp, R. Wegener, Influence of urban air on proton exchange membrane fuel cell vehicles–Long term effects of air contaminants in an authentic driving cycle, J. Power Sources 400 (2018) 556–565.
[90] J.M. Moore, P.L. Adcock, J.B. Lakeman, G.O. Mepsted, The effects of battlefield contaminants on PEMFC performance, J. Power Sources 85 (2) (2000) 254–260.
[91] S. Jiménez, J. Soler, R.X. Valenzuela, L. Daza, Assessment of the performance of a PEMFC in the presence of CO, J. Power Sources 151 (2005) 69–73.
[92] G.J.M. Janssen, Modelling study of CO2 poisoning on PEMFC anodes, J. Power Sources 136 (1) (2004) 45–54.
[93] W. Shi, B. Yi, M. Hou, F. Jing, P. Ming, Hydrogen sulfide poisoning and recovery of PEMFC Pt-anodes, J. Power Sources 165 (2) (2007) 814–818.
[94] M.J. Tierney, H.O.L. Kim, Electrochemical gas sensor with extremely fast response times, Anal. Chem. 65 (23) (1993) 3435–3440.
[95] U. Guth, W. Vonau, J. Zosel, Recent developments in electrochemical sensor application and technology—a review, Meas. Sci. Technol. 20 (4) (2009), 042002.
[96] G. Bidan, Electroconducting conjugated polymers: new sensitive matrices to build up chemical or electrochemical sensors, A review. Sensors and Actuators B: Chemicals 6 (1–3) (1992) 45–56.
[97] P. Barritault, M. Brun, O. Lartigue, J. Willemin, J.L. Ouvrier-Buffet, S. Pocas, S. Nicoletti, Low power CO2 NDIR sensing using a micro-bolometer detector and a micro-hotplate IR-source, Sensor. Actuator. B Chem. 182 (2013) 565–570.
[98] T.V. Dinh, I.Y. Choi, Y.S. Son, J.C. Kim, A review on non-dispersive infrared gas sensors: improvement of sensor detection limit and interference correction, Sensor. Actuator. B Chem. 231 (2016) 529–538.
[99] T. Lillesand, R.W. Kiefer, J. Chipman, Remote Sensing and Image Interpretation, John Wiley & Sons, 2015.
[100] A. Sklorz, S. Janßen, W. Lang, Detection limit improvement for NDIR ethylene gas detectors using passive approaches, Sensor. Actuator. B Chem. 175 (2012) 246–254.
[101] X. Jia, J. Roels, R. Baets, G. Roelkens, On-chip non-dispersive infrared CO2 sensor based on an integrating cylinder, Sensors 19 (19) (2019) 4260.
[102] T.A. Vincent, J.W. Gardner, A low cost MEMS based NDIR system for the monitoring of carbon dioxide in breath analysis at ppm levels, Sensor. Actuator. B Chem. 236 (2016) 954–964.
[103] R. Moos, K. Sahner, M. Fleischer, U. Guth, N. Barsan, U. Weimar, Solid state gas sensor research in Germany–a status report, Sensors 9 (6) (2009) 4323–4365.
[104] P.T. Moseley, Solid state gas sensors, Meas. Sci. Technol. 8 (3) (1997) 223.
[105] A.M. Azad, S.A. Akbar, S.G. Mhaisalkar, L.D. Birkefeld, K.S. Goto, Solid-state gas sensors: a review, J. Electrochem. Soc. 139 (12) (1992) 3690.

[106] Y.F. Sun, S.B. Liu, F.L. Meng, J.Y. Liu, Z. Jin, L.T. Kong, J.H. Liu, Metal oxide nanostructures and their gas sensing properties: a review, Sensors 12 (3) (2012) 2610–2631.
[107] G. Korotcenkov, Metal oxides for solid-state gas sensors: what determines our choice? Mater. Sci. Eng., B 139 (1) (2007) 1–23.
[108] S.G. Chatterjee, S. Chatterjee, A.K. Ray, A.K. Chakraborty, Graphene–metal oxide nanohybrids for toxic gas sensor: a review, Sensor. Actuator. B Chem. 221 (2015) 1170–1181.
[109] A. Dey, Semiconductor metal oxide gas sensors: a review, Mater. Sci. Eng., B 229 (2018) 206–217.
[110] E.B. Lee, I.S. Hwang, J.H. Cha, H.J. Lee, W.B. Lee, J.J. Pak, B.K. Ju, Micromachined catalytic combustible hydrogen gas sensor, Sensor. Actuator. B Chem. 153 (2) (2011) 392–397.
[111] International Sensor Technology. http://www.intlsensor.com/pdf/catalyticbead.pdf, 2020. (Accessed 10 May 2020).
[112] R.L. Grob, E.F. Barry (Eds.), Modern Practice of Gas Chromatography, vol. 2, Wiley, New York, 1977.
[113] P. Warburton, M. Pagano, R. Hoover, M. Logman, K. Crytzer, Y. Warburton, Amperometric gas sensor response times, Anal. Chem. 70 (5) (1998) 998–1006, 1998.
[114] H. Nazemi, A. Joseph, J. Park, A. Emadi, Advanced micro- and nano-gas sensor technology: a review, Sensors 19 (6) (2019) 1285.
[115] Y.J. Choi, I.S. Hwang, J.G. Park, K.J. Choi, J.H. Park, J.H. Lee, Novel fabrication of an SnO_2 nanowire gas sensor with high sensitivity, Nanotechnology 19 (9) (2008), 095508.
[116] A. Ghosh, C. Zhang, S. Shi, H. Zhang, High temperature CO_2 sensing and its cross-sensitivity towards H_2 and CO gas using calcium doped ZnO thin film coated langasite SAW sensor, Sensor. Actuator. B Chem. 301 (2019) 126958.
[117] Operating Manual, H. P. 5890 Series II and HP 5890 Series II Plus, 2020. http://photos.labwrench.com/equipmentManuals/128-6712.pdf. (Accessed 10 May 2020).
[118] S.S. Hung, H.C. Chang, I.N. Chang, A portable Array-type optical fiber sensing instrument for real-time gas detection, Sensors 16 (12) (2016) 2087.
[119] J. Shao, W. Xie, X. Song, Y. Zhang, A new hydrogen sensor based on SNS fiber interferometer with Pd/WO_3 coating, Sensors 17 (9) (2017) 2144.
[120] F.A.A. Nugroho, R. Eklund, S. Nilsson, C. Langhammer, A fiber-optic nanoplasmonic hydrogen sensor via pattern-transfer of nanofabricated PdAu alloy nanostructures, Nanoscale 10 (44) (2018) 20533–20539.
[121] D. Pawar, S.N. Kale, A review on nanomaterial-modified optical fiber sensors for gases, vapors and ions, Microchimica Acta 186 (4) (2019) 253.
[122] M.B. Gerdroodbary, A. Anazadehsayed, A. Hassanvand, R. Moradi, Calibration of low-pressure MEMS gas sensor for detection of hydrogen gas, Int. J. Hydrogen Energy 43 (11) (2018) 5770–5782.
[123] A.A. Vasiliev, A.V. Pisliakov, A.V. Sokolov, N.N. Samotaev, S.A. Soloviev, K. Oblov, A.S. Lipilin, Non-silicon MEMS platforms for gas sensors, Sensor. Actuator. B Chem. 224 (2016) 700–713.
[124] T.A. Vincent, J.W. Gardner, A low cost MEMS based NDIR system for the monitoring of carbon dioxide in breath analysis at ppm levels, Sensor. Actuator. B Chem. 236 (2016) 954–964.
[125] R. Prajesh, N. Jain, V.K. Khanna, V. Gupta, A. Agarwal, MEMS based integrated gas sensor for NO 2 and NH 3, J ISSS 3 (2) (2014) 1–6.
[126] T. Kawano, H.C. Chiamori, M. Suter, Q. Zhou, B.D. Sosnowchik, L. Lin, An electrothermal carbon nanotube gas sensor, Nano Lett. 7 (12) (2007) 3686–3690.
[127] L. Xu, Z. Dai, G. Duan, L. Guo, Y. Wang, H. Zhou, T. Li, Micro/nano gas sensors: a new strategy towards in-situ wafer-level fabrication of high-performance gas sensing chips, Sci. Rep. 5 (2015) 10507.
[128] D. Candusso, F. Harel, A. De Bernardinis, X. Francois, M.C. Péra, D. Hissel, J. M. Kauffmann, Characterisation and modelling of a 5 kW PEMFC for transportation applications, Int. J. Hydrogen Energy 31 (8) (2006) 1019–1030.
[129] Z. Li, Data-driven Fault Diagnosis for PEMFC Systems, 2014. Doctoral dissertation, Aix-Marseille.
[130] RISE, 2020, in: https://www.ri.se/en/what-we-do/projects/optimizing-production-process-bipolar-plates. (Accessed 30 September 2020).
[131] Fj-composite, 2020, 30.09.2020, https://www.fj-composite.com/en/.
[132] R. Sarrate, F. Nejjari, A. Rosich, Model-based optimal sensor placement approaches to fuel cell stack system fault diagnosis, Fault Detection, Supervision and Safety of Technical Processes Volume# 8| (2012) 96–101. Part# 1.
[133] Z. Zheng, R. Petrone, M.C. Péra, D. Hissel, M. Becherif, C. Pianese, M. Sorrentino, A review on non-model based diagnosis methodologies for PEM fuel cell stacks and systems, Int. J. Hydrogen Energy 38 (21) (2013) 8914–8926.
[134] L. Mao, B. Davies, L. Jackson, Application of the sensor selection approach in polymer electrolyte membrane fuel cell prognostics and health management, Energies 10 (10) (2017) 1511.
[135] L. Mao, L. Jackson, Effect of sensor set size on polymer electrolyte membrane fuel cell fault diagnosis, Sensors 18 (9) (2018) 2777.
[136] R.H. Lin, Z.X. Pei, Z.Z. Ye, C.C. Guo, B.D. Wu, Hydrogen fuel cell diagnostics using random forest and enhanced feature selection, Int. J. Hydrogen Energy 45 (17) (2019) 10523–10535.
[137] FCLAB Research. http://eng.fclab.fr/ieee-phm-2014-data-challenge/, 2020. (Accessed 10 May 2020).
[138] H. Liu, J. Chen, D. Hissel, J. Lu, M. Hou, Z. Shao, Prognostics methods and degradation indexes of proton exchange membrane fuel cells: a review, Renew. Sustain. Energy Rev. 123 (2020) 109721.
[139] R. Ma, T. Yang, E. Breaz, Z. Li, P. Briois, F. Gao, Data-driven proton exchange membrane fuel cell degradation predication through deep learning method, Appl. Energy 231 (2018) 102–115.
[140] Z. Li, Z. Zheng, R. Outbib, Adaptive prognostic of fuel cells by implementing ensemble Echo state Networks in time-varying model space, IEEE Trans. Ind. Electron. 67 (1) (2019) 379–389.
[141] S. Morando, S. Jemei, D. Hissel, R. Gouriveau, N. Zerhouni, Proton exchange membrane fuel cell ageing forecasting algorithm based on Echo State Network, Int. J. Hydrogen Energy 42 (2) (2017) 1472–1480.
[142] K. Chen, S. Laghrouche, A. Djerdir, Degradation prediction of proton exchange membrane fuel cell based on grey neural network model and particle swarm optimization, Energy Convers. Manag. 195 (2019) 810–818.
[143] Y. Wang, B. Seo, B. Wang, N. Zamel, K. Jiao, X.C. Adroher, Fundamentals, materials, and machine learning of polymer electrolyte membrane fuel cell technology, Energy and AI 1 (2020), 100014.
[144] W. Xing, M. Razi, R.M. Kirby, K. Sun, A.A. Shah, Greedy nonlinear autoregression for multifidelity computer models at different scales, Energy and AI 1 (2020), 100012.